LIST OF FIGURES

CHAPTER 2. Imaging guide for tractography of major white matter fiber bundles

By Dr Jerome J Maller

Table of contents

1. Introduction

Most white matter fiber bundles in the brain will be slightly curved or warped in appearance. That is, few are 100% straight. Hence, when reconstructed based of fractional anisotropy colour maps, fibers will not appear as consistently solid colours, but rather, a general colour sometimes merging into other colour mixtures. For example, the CC has a strong right-left orientation towards its midline (thus a bold red colour) but radiates dorso-laterally thus a mixture of red (right-left) and blue (dorso-ventral) to yield an orange hue. Some software packages allow for a tracked fiber bundle to be displayed in a single solid colour.

Many bundles are actually comprised on many smaller bundles merging in and out, or across, bundles. Hence, some long bundles e.g. SLF, may not be able to be tracked as a single bundle. Furthermore, resolving crossing fibers becomes more difficult as the data becomes more anisotropic and of lower resolution: this is because we aim to have no more than one fiber passing through each voxel; when a voxel contains 2 or more fiber bundles, they cannot be resolved (and it is common opinion that each voxel, even at 2mm isotropic, will contain fibers from at least 3 different bundles).

Regarding acquisition of the diffusion tensor imaging data, I suggest at least 31 directions of a slice thickness no greater than 3mm. Although $1mm^3$ isotropic would be ideal, the time required to acquire data of such high resolution would be unfeasible for most studies. Currently, many studies are acquiring voxels at $2mm^3$ isotropic resolution. Increasing the number of acquisitions improves SNR and hence the tractography as well. Aim to acquire 1 bzero (no diffusion) volume for every 6 diffusion volumes. Whilst a B value of 1000 s mm^{-2} is suffice, 2000 s mm^{-2} will allow more fibers to be revealed. I highly recommend the article by Jones and Cercignani (2010) which describes 25 pitfalls in the analysis of diffusion MRI data.

2. Region Of Interest (ROI) Placement

Typically, fiber tracking limits are set to angles of between 25 and 75 degrees. Placement of a single Region Of Interest (ROI) is often sufficient to extract a fiber bundle, but often some of the tracked fibers will not be part of the required bundles, hence those voxels will need to be manually deleted. Additionally, sometimes part of a fiber bundle will not be tracked due to limited resolution (for example), hence that part of the fiber bundle will need to be tracked separately.

3. Major white matter fiber bundles of the human brain

Here are some figures illustrating the trajectories of the major white matter bundles in the human brain:

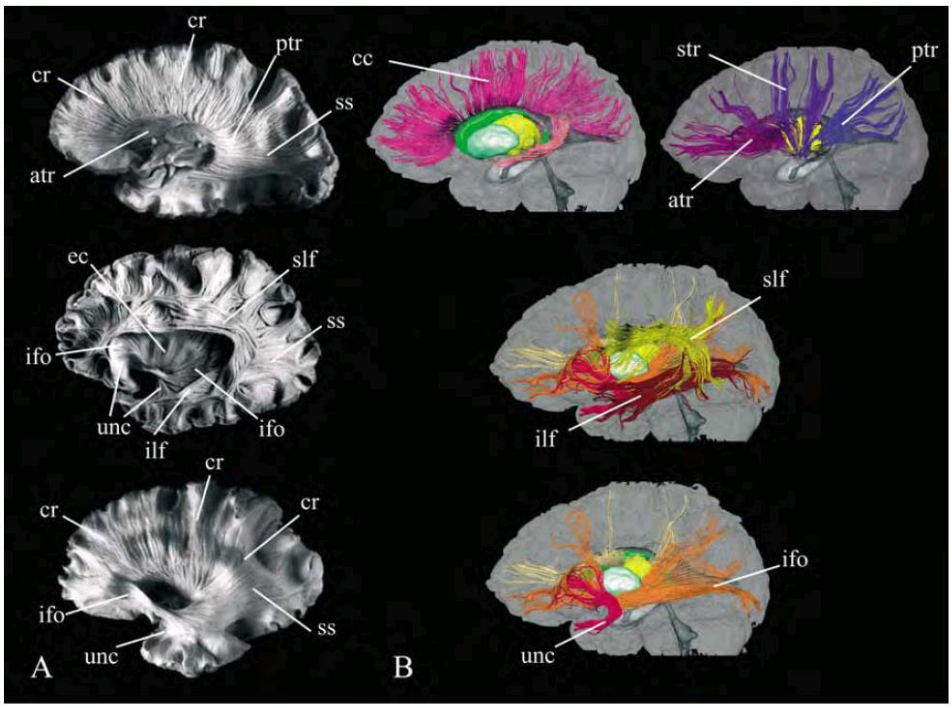

Figure 58. Comparison between postmortem preparation (A) and DTI-based reconstruction results (B). Abbreviations are atr: anterior thalamic radiation; cc: corpus callosum; cr: corona radiata; ec: external capsule; ifo: inferior fronto-occipital tract; ilf: inferior longitudinal fasciculus; ptr: posterior thalamic radiation; ss: sagittal stratum; slf: superior longitudinal fasciculus; str: superior thalamic radiation; unc: uncinate fasciculus. Copyright protected material (postmortem tissue images) used with permission of the authors and the University of Iowa's Virtual Hospital, www.vh.org (Mori et al., 2005).

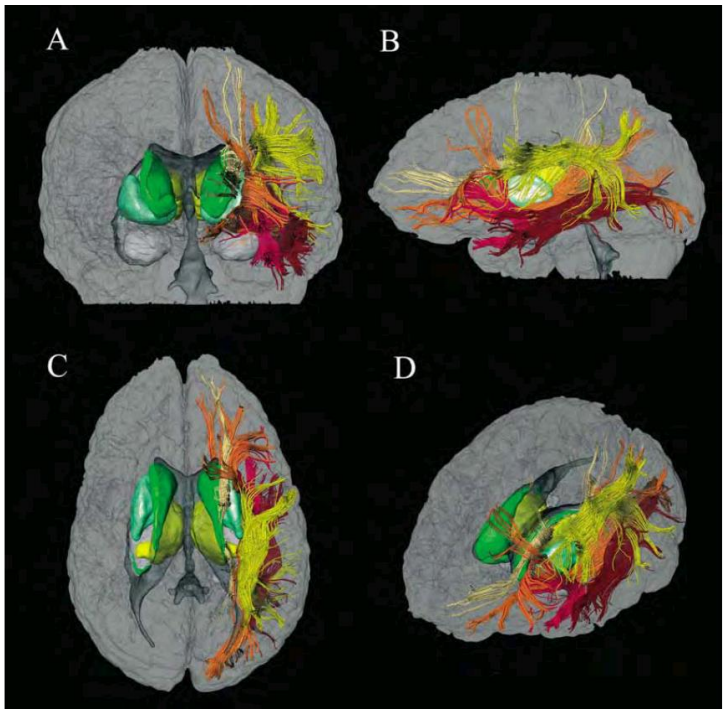

Figure 59. 3D reconstruction results of some association fibers. Tracts are viewed from the anterior (A), left (B), superior (C), and oblique (left-antero-superior) (D) orientations. Color coding: SLF is yellow, IFOF is orange, UF is red and ILF is brown. Cerebral hemispheres are delineated by semi-transparent (Mori et al., 2005).

3(i). Superior Longitudinal Fasciculus (SLF)

The SLF is composed of four distinct components: SLF I, SLF II, SLF III, and arcuate fascicle (AF), although current resolution restricts this to the identification of 1 large SLF bundle. DSI (diffuse spectrum imaging) can identify these separately but a spatial resolution of around 512 micron is required, acquired at 4.7T or above (Figure 60).

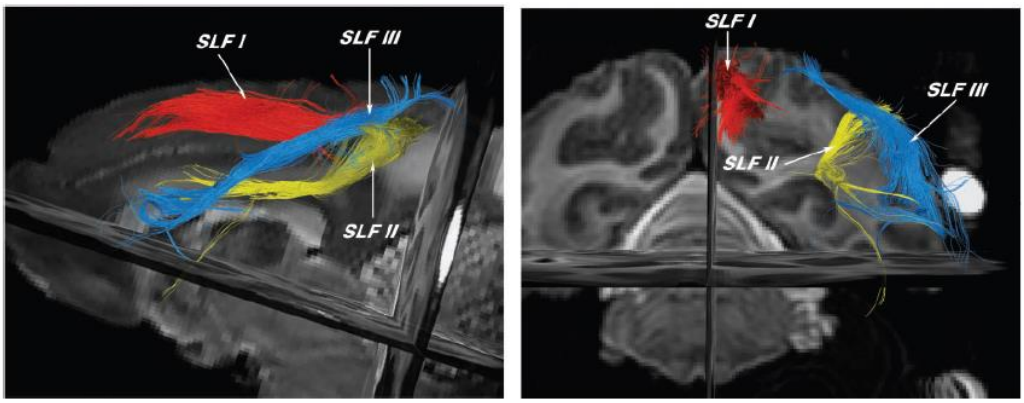

Figure 60. SLF I, II, III from DSI of a monkey brain (25 hrs scanning time; Schmahmann et al., 2007).

The SLF is best tracked from a single ROI located at the temporo-parietal junction just before it curves ventrally. At this point the bundle is green (Figure 61, #1).

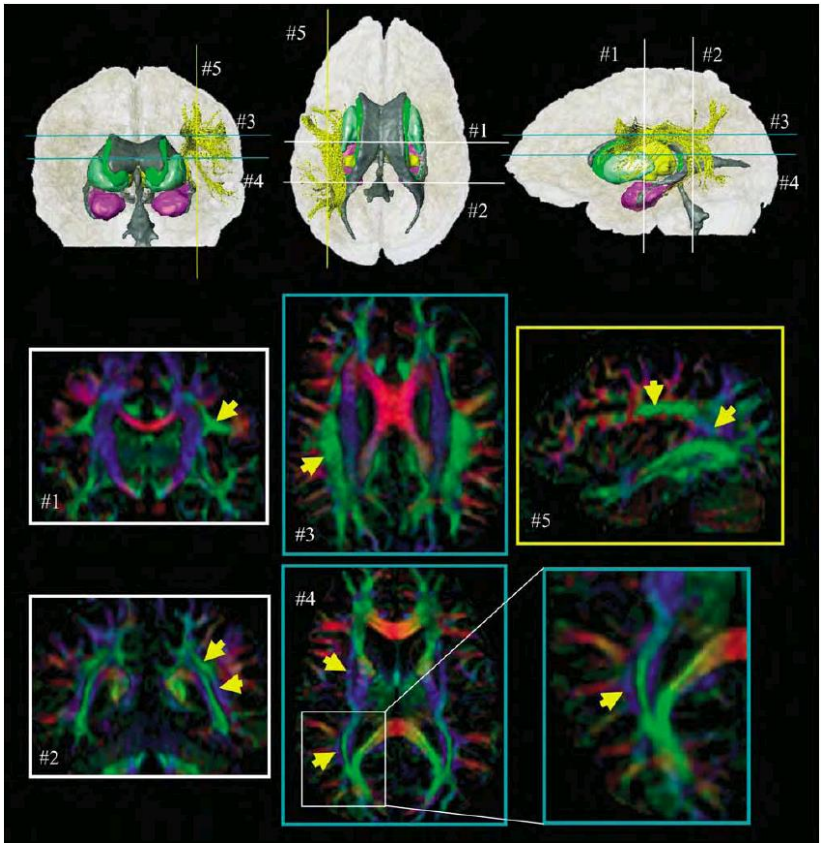

Figure 61. The trajectory of the SLF and its identification in the color maps at various slice levels and orientations. Locations of 2D slices are indicated in the 3D panels. The hippocampus and amygdala (purple), thalamus (yellow), ventricular system (gray), caudate (green), and putamen (light green) are also shown in the 3D reconstruction (Mori et al., 2005).

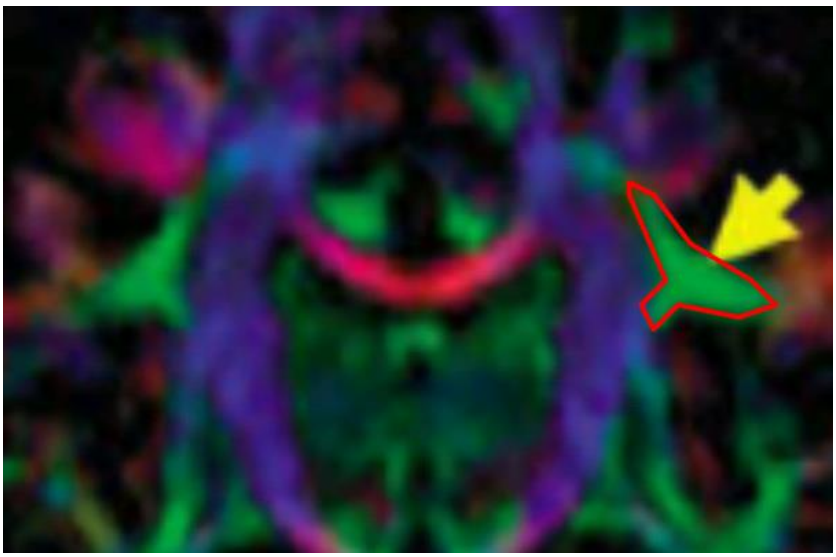

Figure 62. ROI placement (**red border**) for tracking of the SLF.

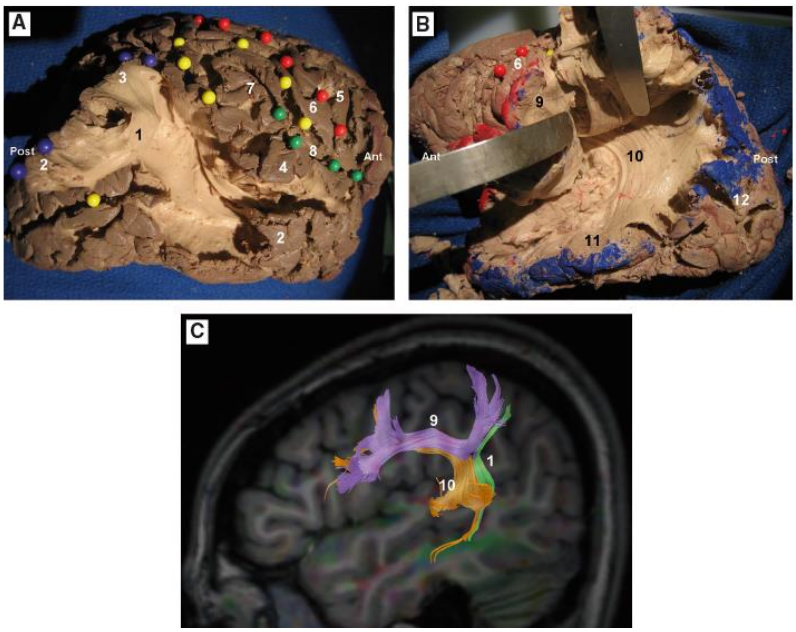

Figure 63. Cortex-sparing fiber dissection of the SLF. (A) Fiber dissection of the vertical segment of the SLF in a right hemisphere. The tract has been tilted and separated from the deeply located AF. Red spheres mark the central sulcus, yellow spheres mark the intraparietal sulcus and the intermediate sulcus of Jensen, green spheres mark the Sylvian fissure, and blue spheres mark the cortical connections of the vertical segment of the SLF. (B) In this left hemisphere the horizontal segment of the SLF has been tilted and separated from the deeply located AF. (A and B). The isolated tracts with preservation of brain structure. (C) DTI tractography reconstruction of the three components of the SLF in a left hemisphere. 1, vertical segment of the SLF; 2, middle temporal gyrus; 3, angular gyrus; 4, superior temporal gyrus; 5, precentral gyrus; 6, postcentral gyrus; 7, supramarginal gyrus; 8, sylvian fissure; 9, horizontal segment of the SLF; 10, AF; 11, inferior temporal gyrus; 12, occipital lobe. Ant, anterior; Post, posterior. of SLF and AF (Martino et al., 2011).

3 (ii). Corticospinal (thalamocortical)

In essence, we need to identify the anterior and posterior limbs of the internal capsule. As the posterior limb is largely in a ventral-dorsal direction, it will be mostly a rich blue in colour. From axial, it is represented by the tracts pointing medially at around 45 degrees (anterior-posterior), and from

coronal it appears as the large bundle travelling at around 10 to 20 degrees lateral to the lateral ventricles. From sagittal, it appears as a thick bundle/radiation travelling on a slight angle posteriorly.

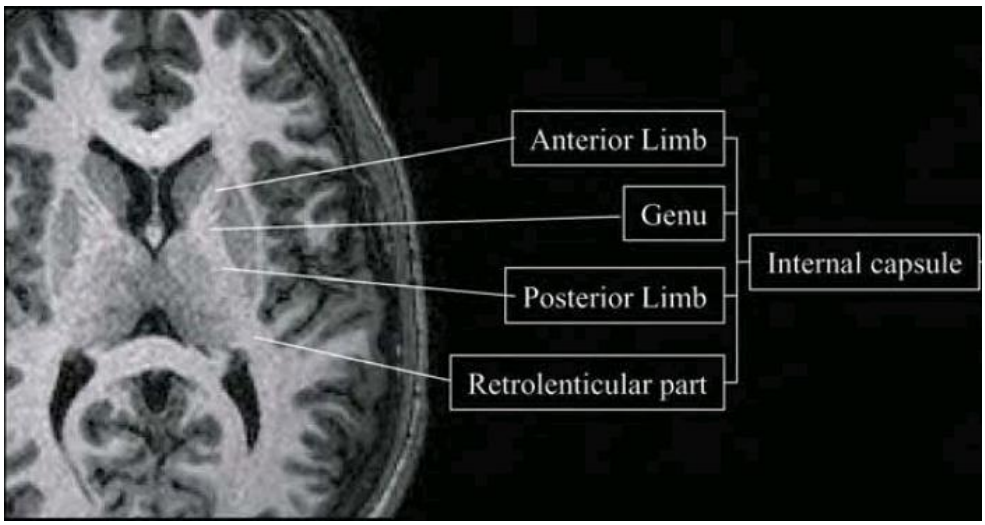

Figure 64. Relationship between various nomenclatures of white matter tracts in the internal capsule. Names in the left column are related to anatomical locations while those in the right column are connectivity-based (Mori et al., 2005).

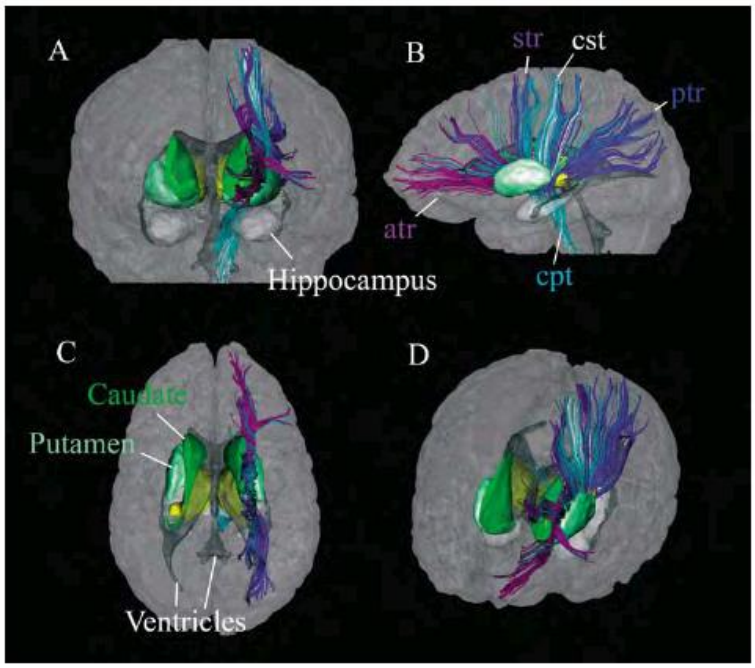

Figure 65. 3D reconstruction results of projection fibers. Tracts are viewed from the anterior (A), left (B), superior (C), and oblique (left-superior-anterior) (D) orientations. The hemispheres are delineated in semi-transparent gray. Abbreviations are: atr: anterior thalamic radiation; cpt: corticopontine tract; cst: corticospinal tract; ptr: posterior thalamic radiation; str: superior thalamic radiation (Mori et al., 2005).

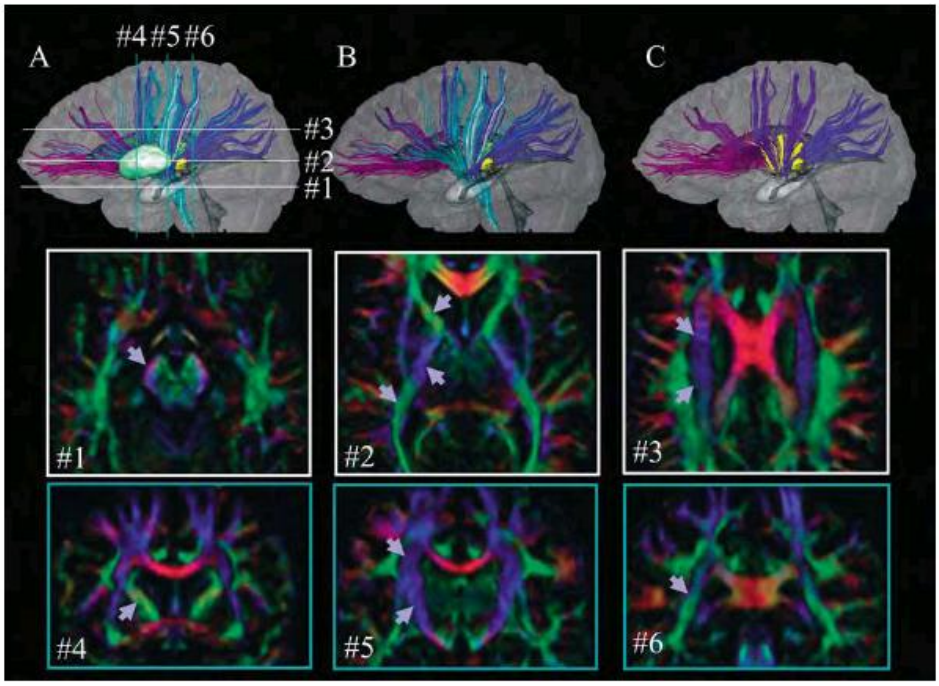

Figure 66. 3D reconstruction results of the projection fibers (A–C). In (B), the putamen was removed to better visualize the tracts, and in (C), the corticopontine (light blue) and corticospinal (white) tracts were removed for better assessment of the thalamic radiations. Locations of the projection tracts are indicated by purple arrows in the 6 color maps (Mori et al., 2005).

3(iii). Optic radiation

The posterior thalamic radiation should include the optic radiation, which connects the lateral geniculate nucleus and the occipital lobe. Although these three components of the thalamic radiation are differently color-coded in this reconstruction, there is no precise distinction between the anterior and superior or superior and posterior thalamic radiations and, thus, their boundaries should not be considered as definite for assignment of these fibers (Mori et al., 2005). The best seeds are the lateral geniculate nuclei, sagittal stratums, and Bands of Gennari.

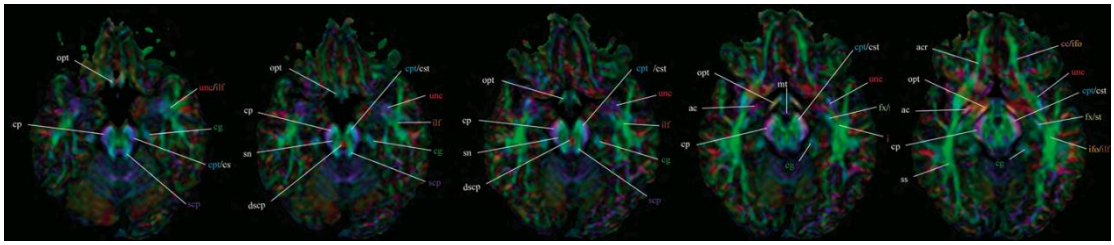

Figure 67. Axial trajectory of the optic radiation from ventral (left) to dorsal (right; Mori et al., 2005).

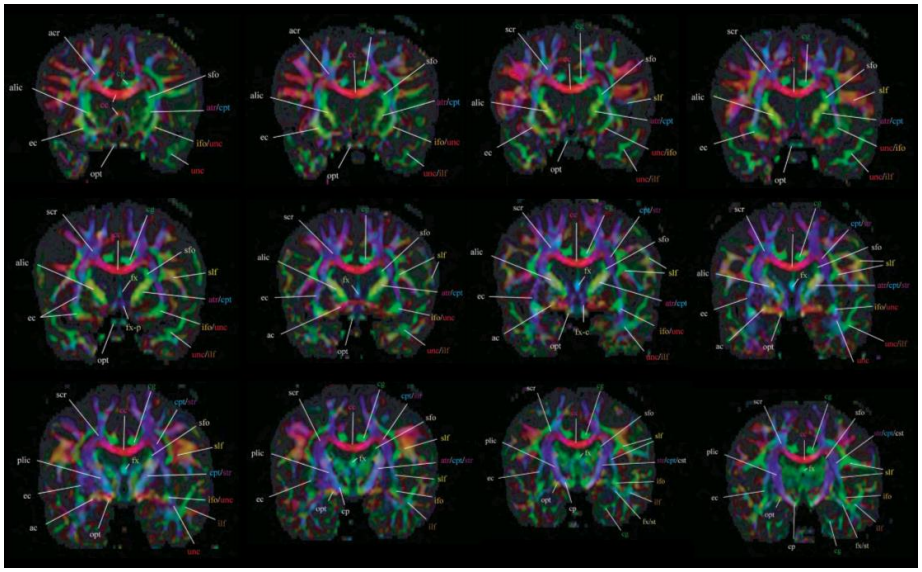

Figure 68. Coronal trajectory of the optic radiation from anterior to posterior (top left to right, middle left to right, bottom left to right; Mori et al., 2005).

3(iv). Corpus callosum (CC)

From coronal, the CC is boldly left-red across the midline and then curves tightly to become ventral-dorsal in orientation (Figure 68). Note that some people exclude the tapetum. The initial ROI for CC tracking is best placed along the midsagittal slice (Figure 89b).

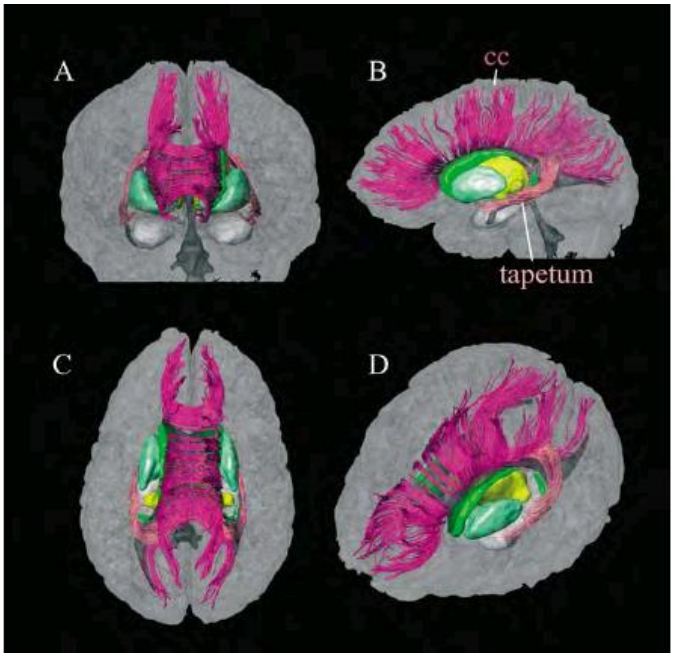

Figure 69. 3D reconstruction results of commissural fibers. Tracts are viewed from the anterior (A), left (B), superior (C), and oblique (left-antero-superior) (D) orientations. Color coding is magenta representing the CC, and peach representing the tapetum (Mori et al., 2005).

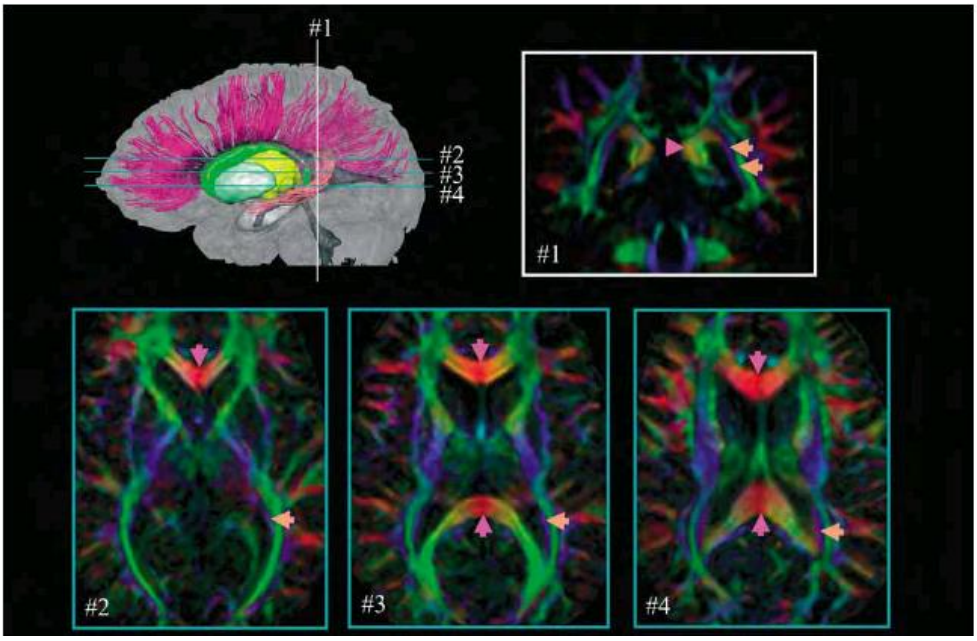

Figure 70. Trajectories of the CC (magenta) and tapetum (peach) and their identification in color maps at various slice levels and orientations. Locations of the 2D slices are indicated in the 3D panel. Note the thalamus (yellow) and ventricular system (Mori et al., 2005).

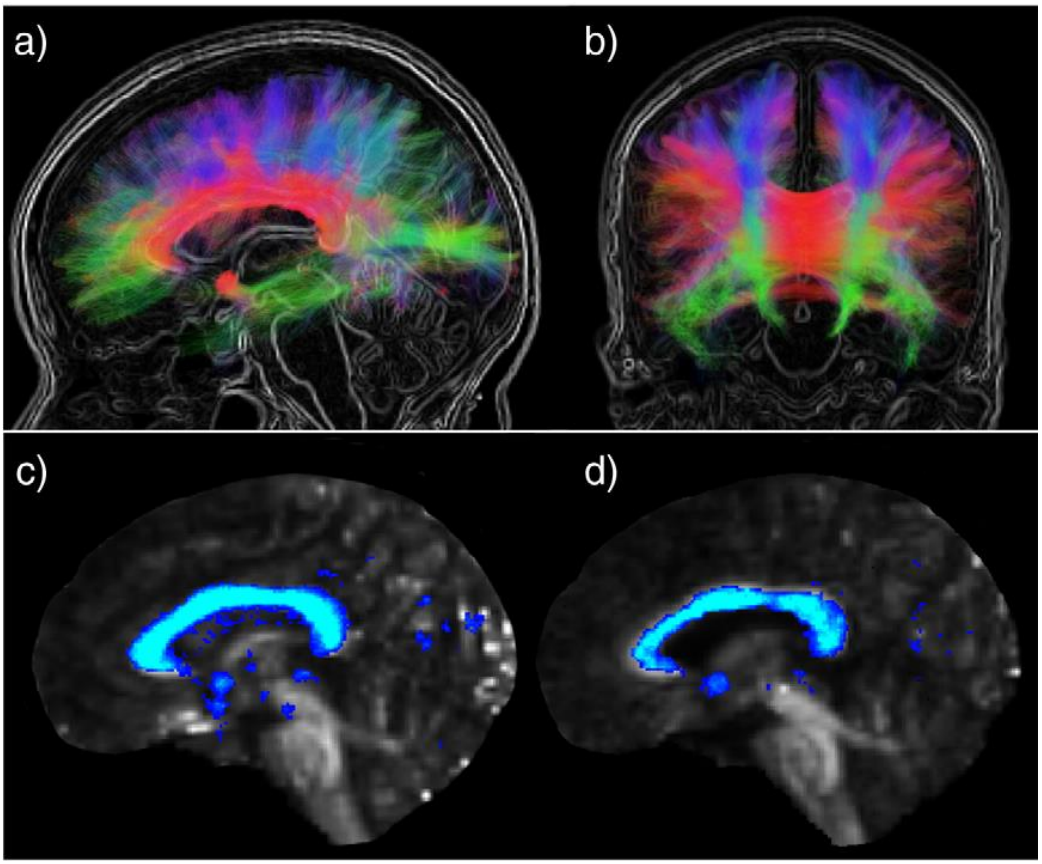

Figure 71. (a & b) Representative commissural streamlines extracted from the b=3000 s mm^{-2} HARDI dataset, overlaid on the individual's structural MRI. Visitation maps for these streamlines generated using the (c) b=1000 s mm^{-2} dataset, and (d) the b=3000 s mm^{-2} dataset are also shown overlaid on the individual FA maps (Pannek et al., 2010).

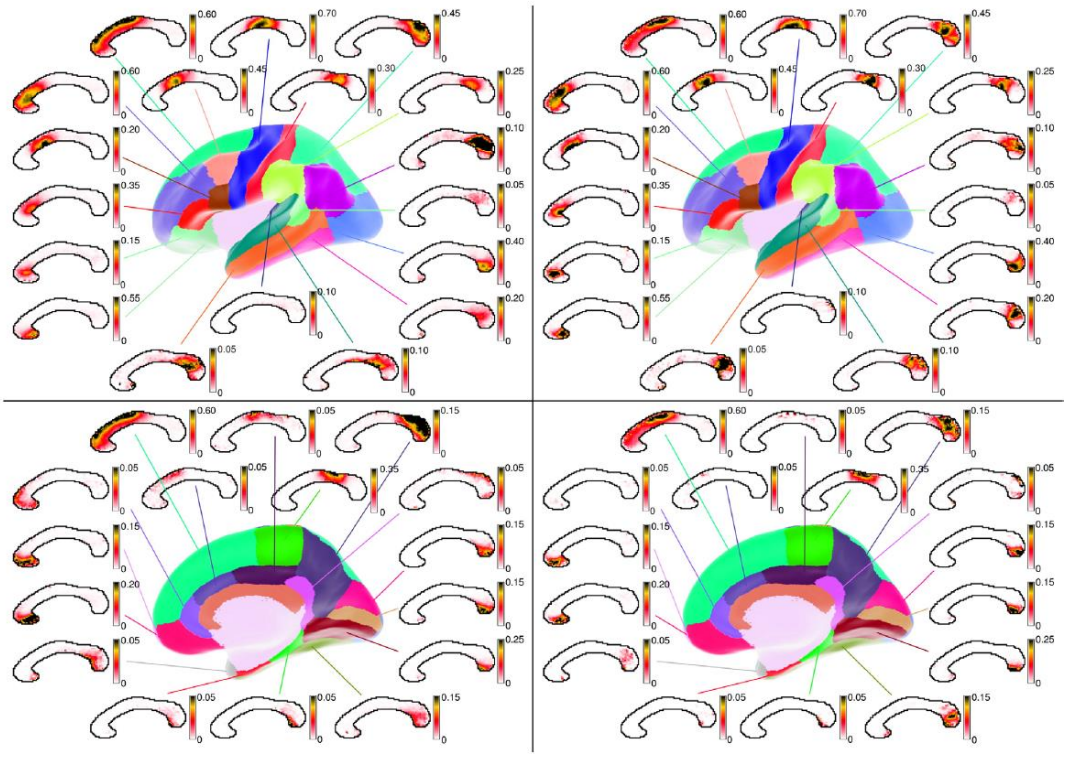

Figure 72. Probabilistic CC population maps, averaged across 8 healthy participants. Results obtained from the low b-value diffusion data are displayed on the left; results obtained from the high b-value diffusion data are displayed on the right. The top panel shows the lateral cortical surface, while the bottom panel shows the medial cortical surface. Each callosal map is connected with its corresponding cortical region via a line of the same colour as the cortical target on the 3D surface. The colour bar shows the probability scale (Pannek et al., 2010).

3(v). Inferior longitudinal fasciculus (ILF) and Inferior fronto-occipital fasciculus (IFOF)

The ILF and IFOF are very difficult to separate based on DTI at currently acquired resolution (Mori et al., 2005). Hence, they are tracked as a single fiber bundle (Figure 73).

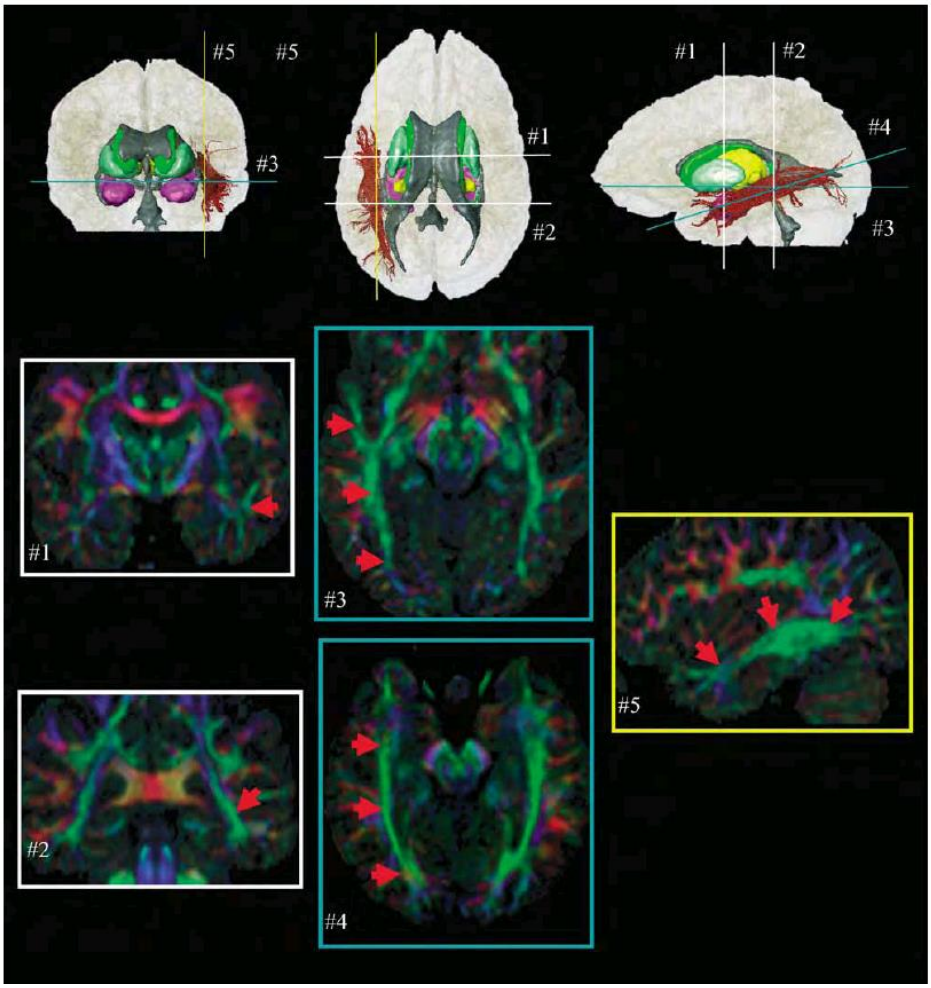

Figure 73. The trajectory of the ILF and its identification in color maps at various slice levels and orientations. Locations of the 2D slices are indicated in the 3D panels. The hippocampus and amygdala (purple), thalamus (yellow), ventricular system (gray), caudate (green), and putamen (light green) are also shown in the 3D reconstruction (Mori et al., 2005).

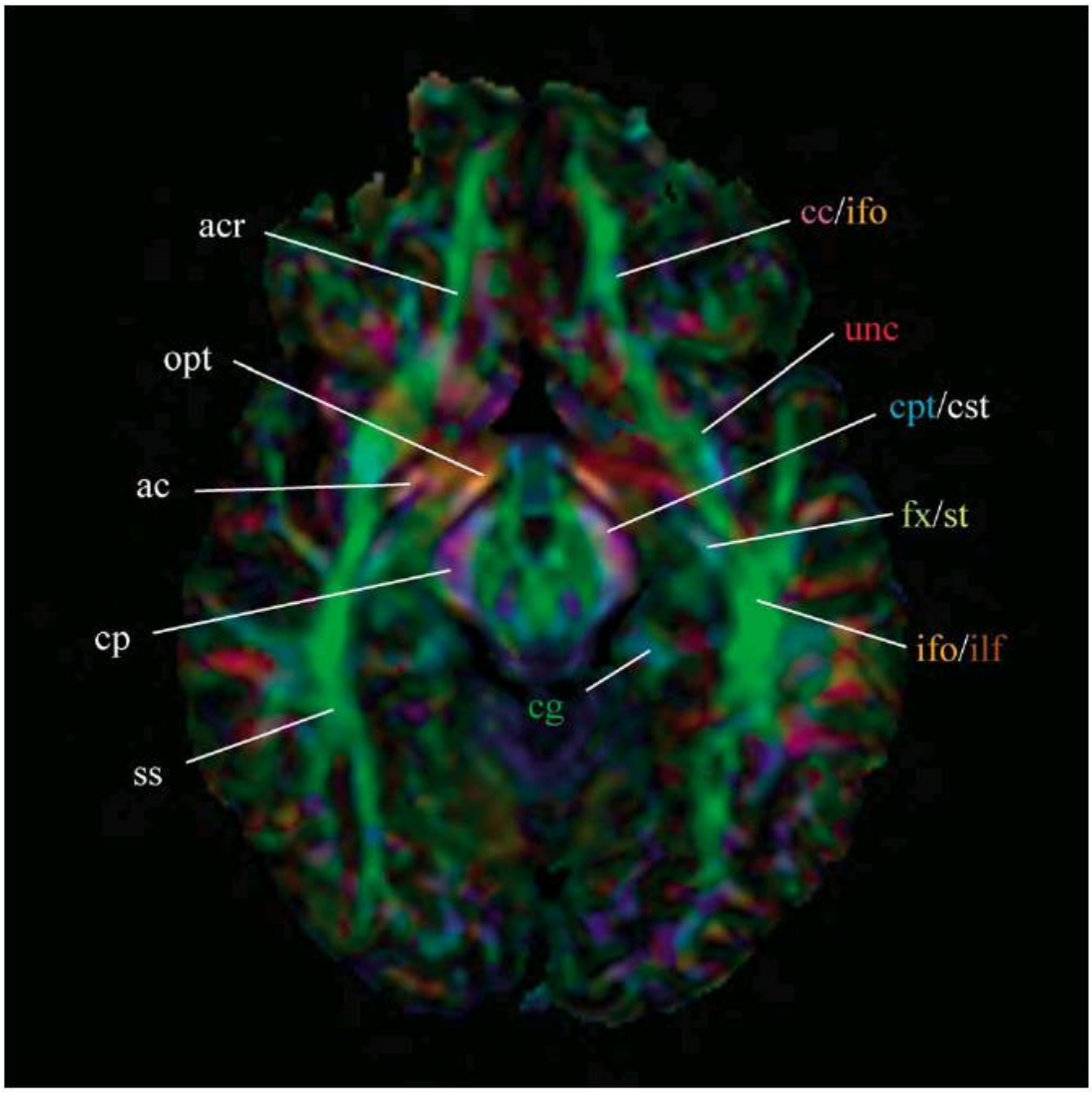

ac: anterior commissure
acr: anterior corona radiata
cc: corpus callosum
cg: cingulum
cp: cerebral peduncle
cpt: corticopontine tract
cst: corticospinal tract
fx: fornix
ifo: inferior fronto-occipital fasciculus
ilf: inferior longitudinal fasciculus
opt: optic tract
ss: sagittal stratum
st: stria terminalis
unc: uncinate fasciculus

Figure 74. IFO-ILF (Mori et al., 2005)

3(vi). Arcuate fasciculus (AF)

The AF (Latin, “curved bundle”) originates in the caudal area of the superior temporal gyrus and passes next to the neurons of SLF II above the Sylvian fissure and insula in non-human primates. In humans, neurons that originate from the caudal superior temporal gyrus and the superior temporal

sulcus pass around the caudal Sylvian fissure and along with the SLF bundle and terminate in the dorsal prefrontal cortex.

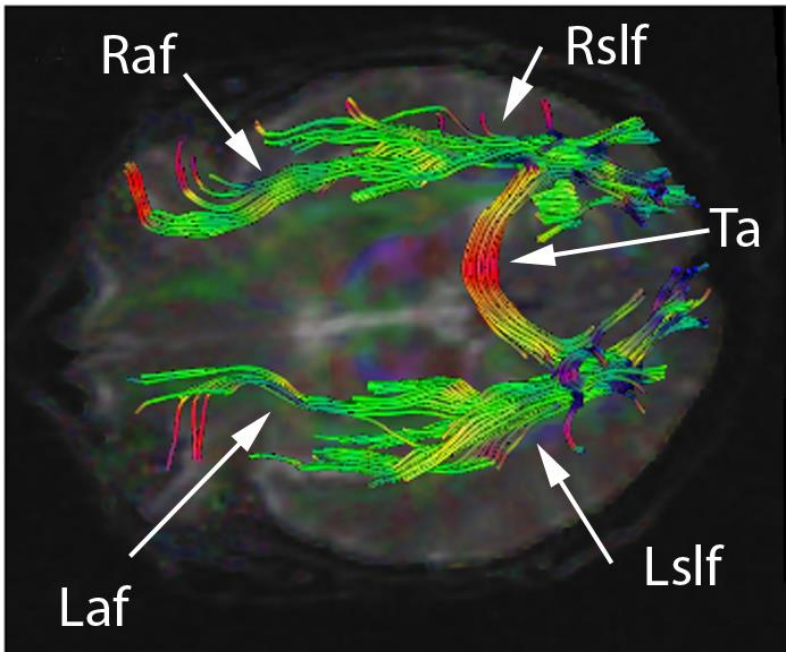

Figure 75. Relationship between AF and SLF. From Aaron G. Filler (2009).

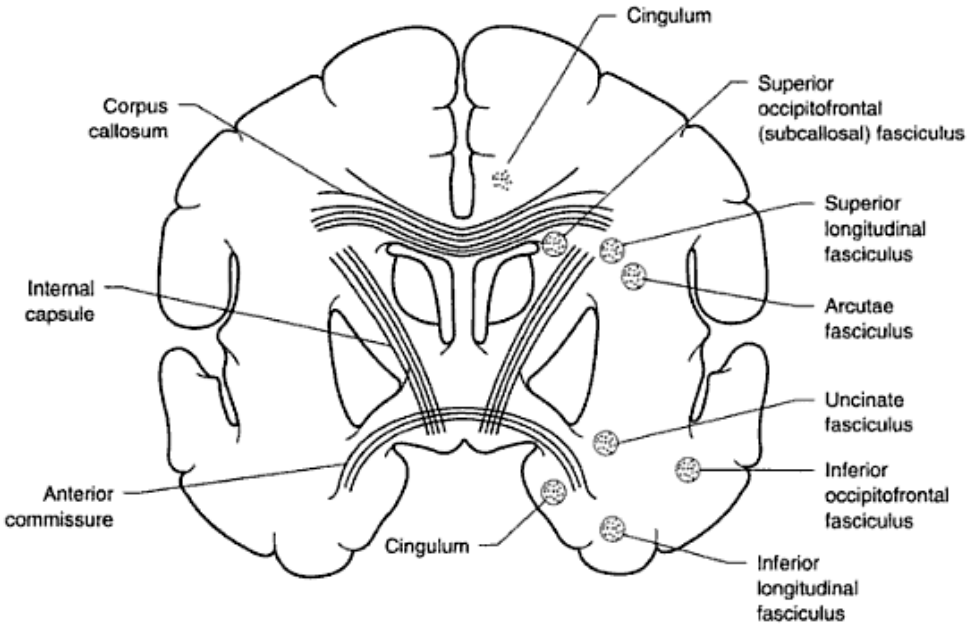

Figure 76. Coronal view demonstrating major association, commissural, and projection fiber systems, and the location of the SLF relative to the AF. From DeJong's (2005) *The neurologic examination*.

Kaplan et al. (2010) tracked the AF in the following manner:

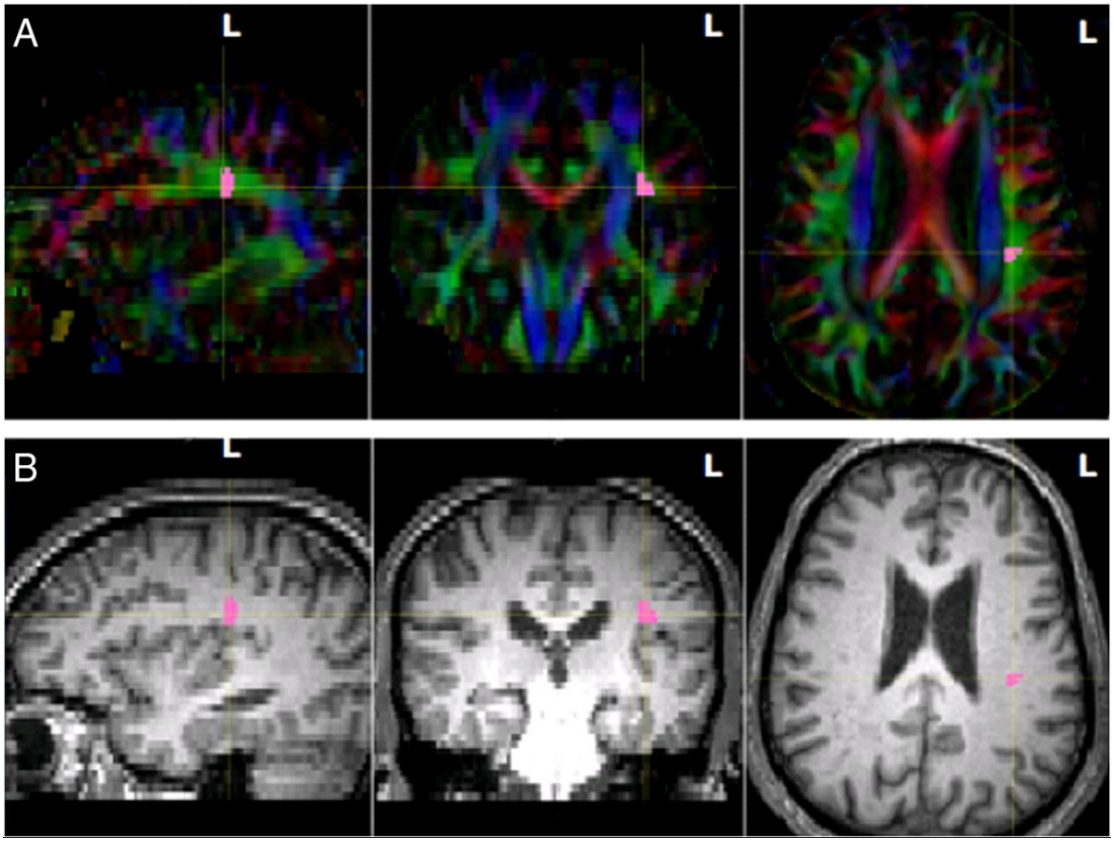

Figure 77. Method used for locating the hAF seed point (pink) in sagittal, coronal and axial views in the LH (subject N4). The hAF seed point was drawn on 5–7 coronal slices in the hAF fibers oriented in the anterior–posterior direction (green). The AF seed point was located superior to the insula, extreme capsule, claustrum, external capsule, and internal capsule. A similar hAF seed point was drawn in the RH (not shown). (A) FA Color Maps; (B) Structural MRI Images. Abbreviations: hAF, horizontal mid-portion of the arcuate fasciculus; LH, left hemisphere; RH, right hemisphere (Kaplan et al., 2010).

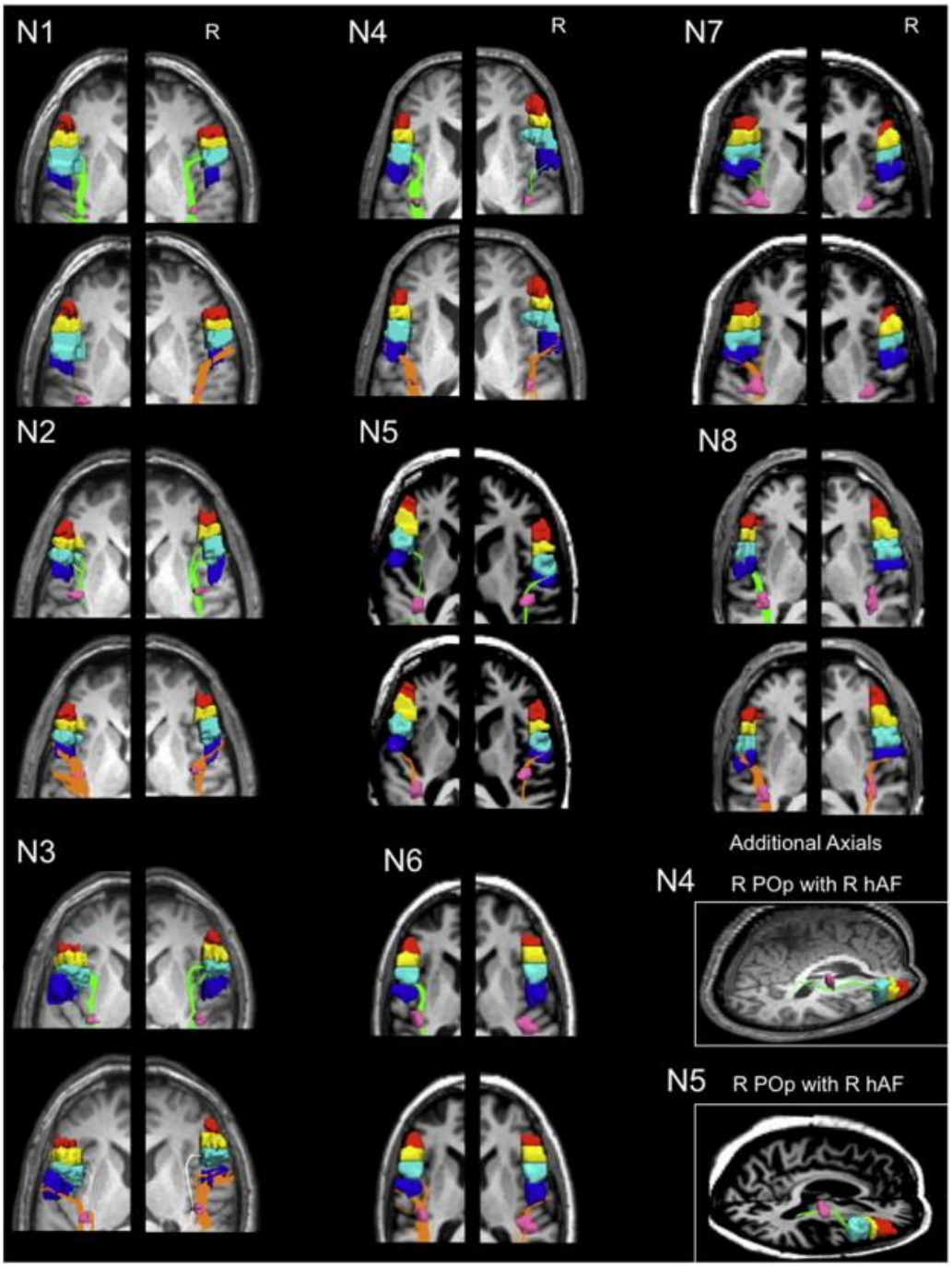

Figure 78. Fiber tracts between the hAF seed point (pink) and the separate cortical ROI seed points in the LH and RH for each subject. The cortical seed points are anterior PTr (red); posterior PTr (yellow); POp (light blue); and vPMC (dark blue). The fiber tracts between hAF and POp are shown in green; and those between hAF and POp, orange. Fiber tracts between hAF and posterior PTr (present only in N3) are shown in white (shown on the same slice as those for vPMC, to conserve space; tractography was performed separately between hAF and each cortical ROI seed point). There were no fiber tracts between hAF and A-PTr in either hemisphere for any subjects. Additional axial views are provided for subjects N4 and N5, showing fiber tracts between the hAF and R POp, where view of R POp was obscured by the presence of R vPMC on other axial views above, for these two subjects. Abbreviations: hAF, horizontal, mid-portion arcuate fasciculus; POp, pars opercularis; PTr, pars triangularis; vPMC, ventral premotor cortex (Kaplan et al., 2010).

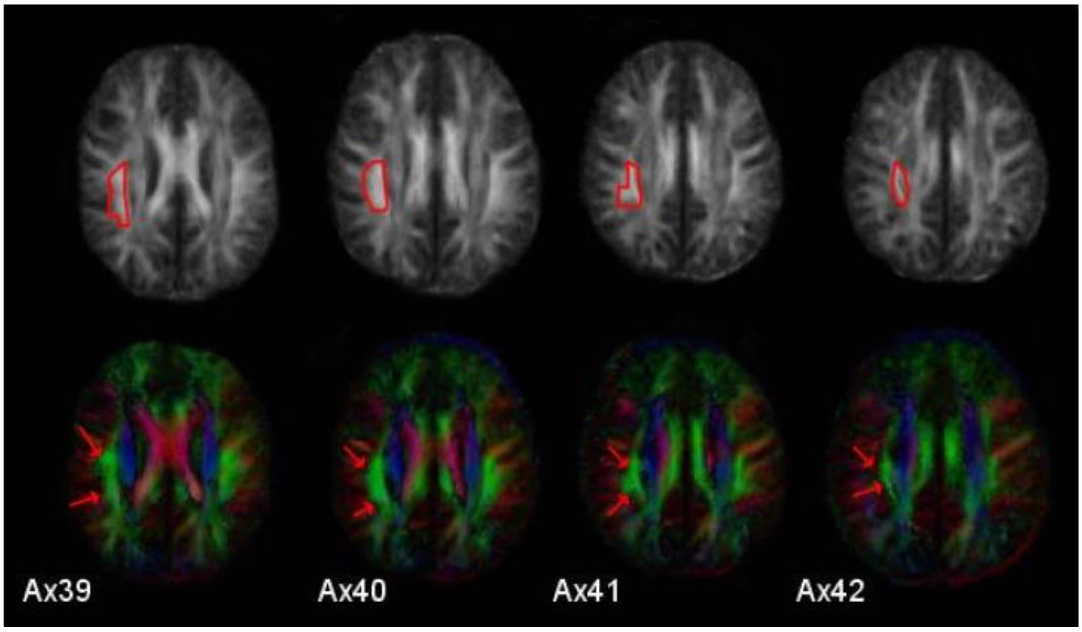

Figure 79. Demarcation of the ROI around the AF in the right hemisphere. The lower row presents axial color fibre orientation maps from a single subject (Talairach z = 39–42). The standard color coding for fiber orientation is used (red: lateral-to-lateral; green: anterior-posteriorly or vice versa; blue: superior-inferiorly or vice versa). Red arrows indicate the extension of the homologues of the AF. According to this color fiber orientation map, a ROI (encircled in red) is defined in the FA image (upper row; Gharabaghi et al., 2009).

3(vii). Uncinate fasciculus (UF)

The UF connects the anterior temporal lobe (including the hippocampal formation) to the orbital cortex.

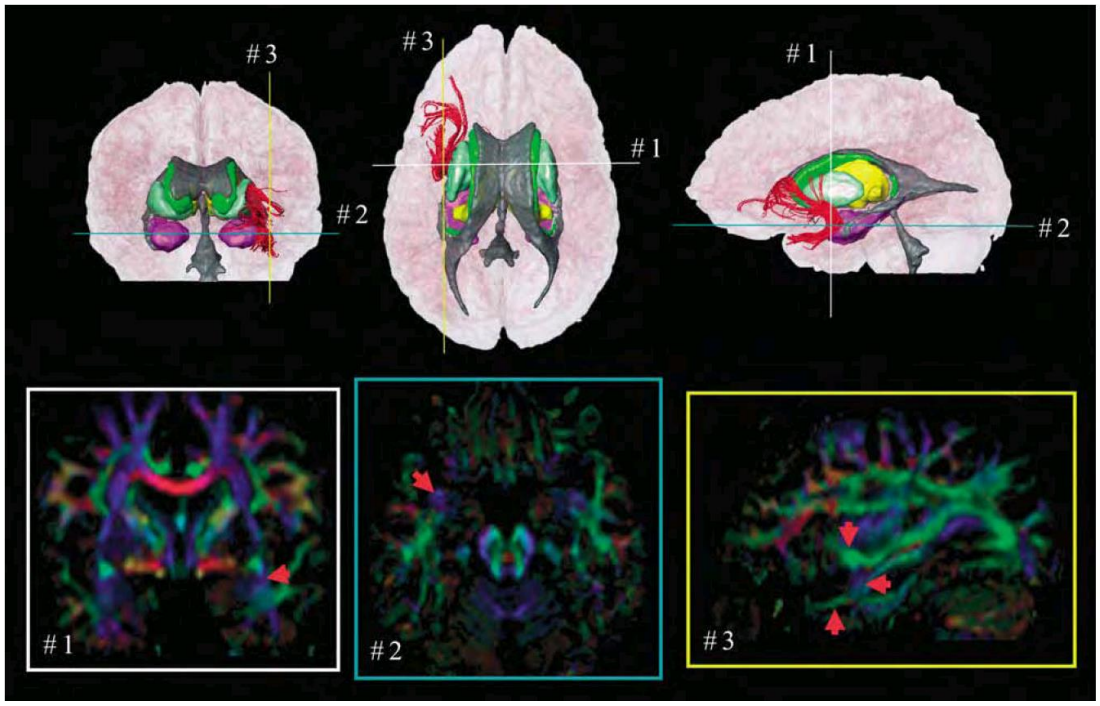

Figure 80. The trajectory of the UF and its identification in color maps at various slice levels and orientations. Locations of the 2D slices are indicated in the 3D panels. The hippocampus and amygdala (purple), thalamus (yellow), ventricular system (gray), caudate (green), and putamen (light green) are also shown in the 3D reconstruction. (Mori et al., 2005).

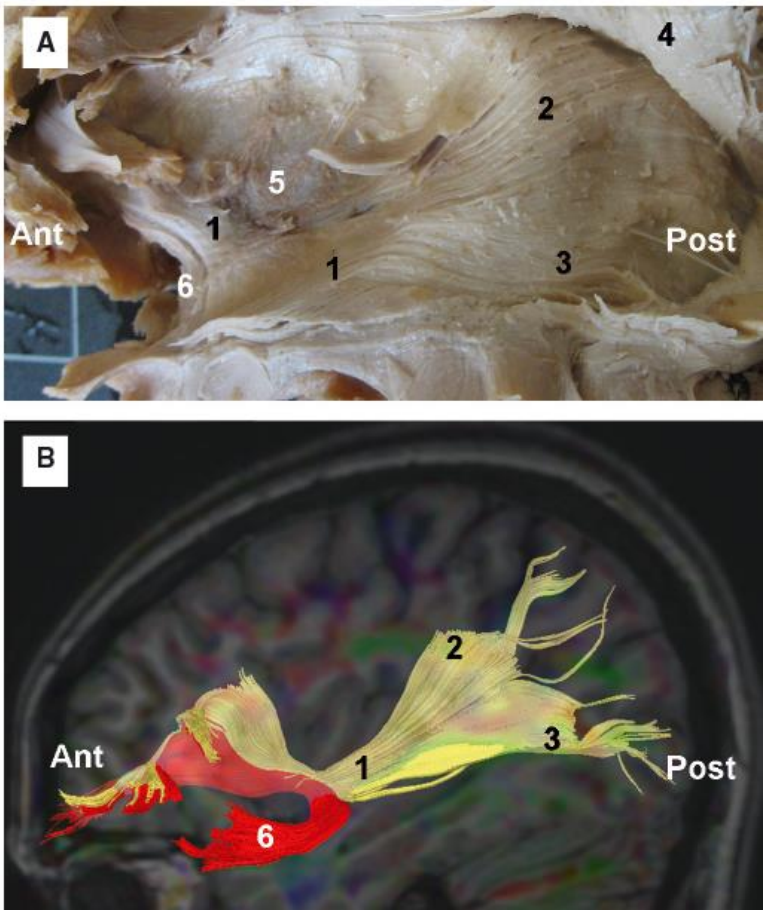

Figure 81. (A) Fiber dissection of the IFOF in a left hemisphere. (B) DTI tractography reconstruction of the IFOF and UF in a left hemisphere. 1, IFOF; 2, fibers of the IFOF connecting with the superior parietal lobe; 3, fibers of the IFOF connecting with the occipital and temporal lobe; 4, AC tilted superiorly; 5, claustrum; 6, UF. Ant, anterior; Post, posterior. (Martino et al., 2011).

3(viii). Cingulate bundle (CB)

The CB are bilateral tracts extending around the entire dorsal and anterior extent of the CC. Hence, most of the CBs traverse in the anterior-posterior direction.

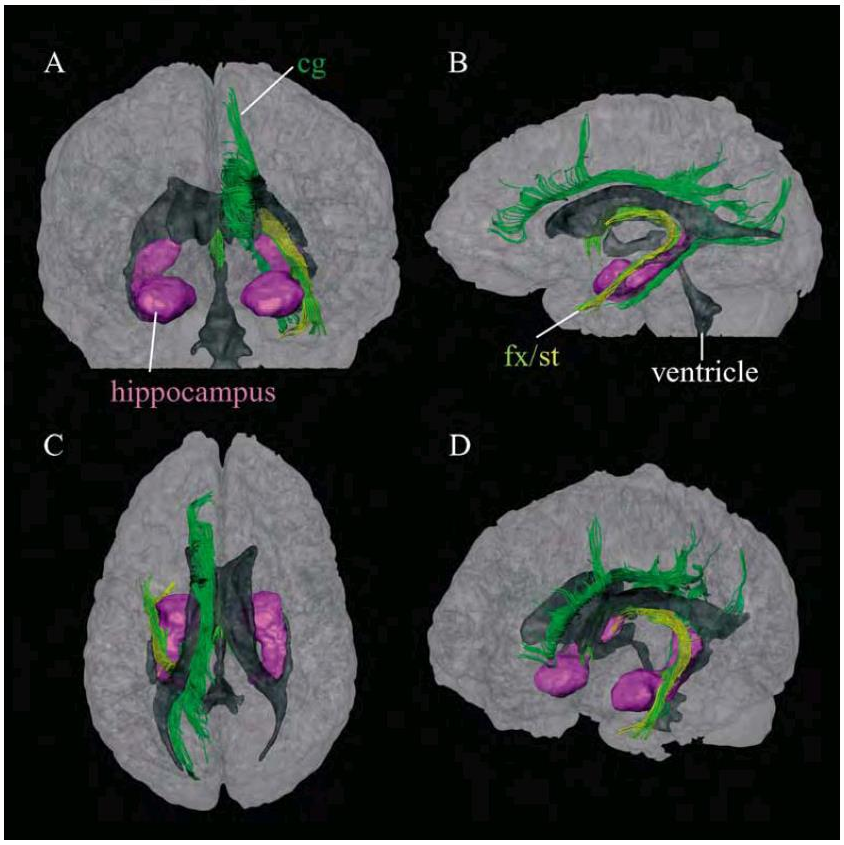

Figure 82. 3D reconstruction results of association fibers in the limbic system. Tracts are viewed from the anterior (A), left (B), superior (C), and oblique (left-anterior) (D) orientations. Abbreviations are: cg: cingulum; fx: fornix, and st: stria terminalis. The cerebral hemispheres are delineated in semi-transparent gray. The ventricular system is depicted in gray and the hippocampi and amygdalae, in purple (Mori et al., 2005)

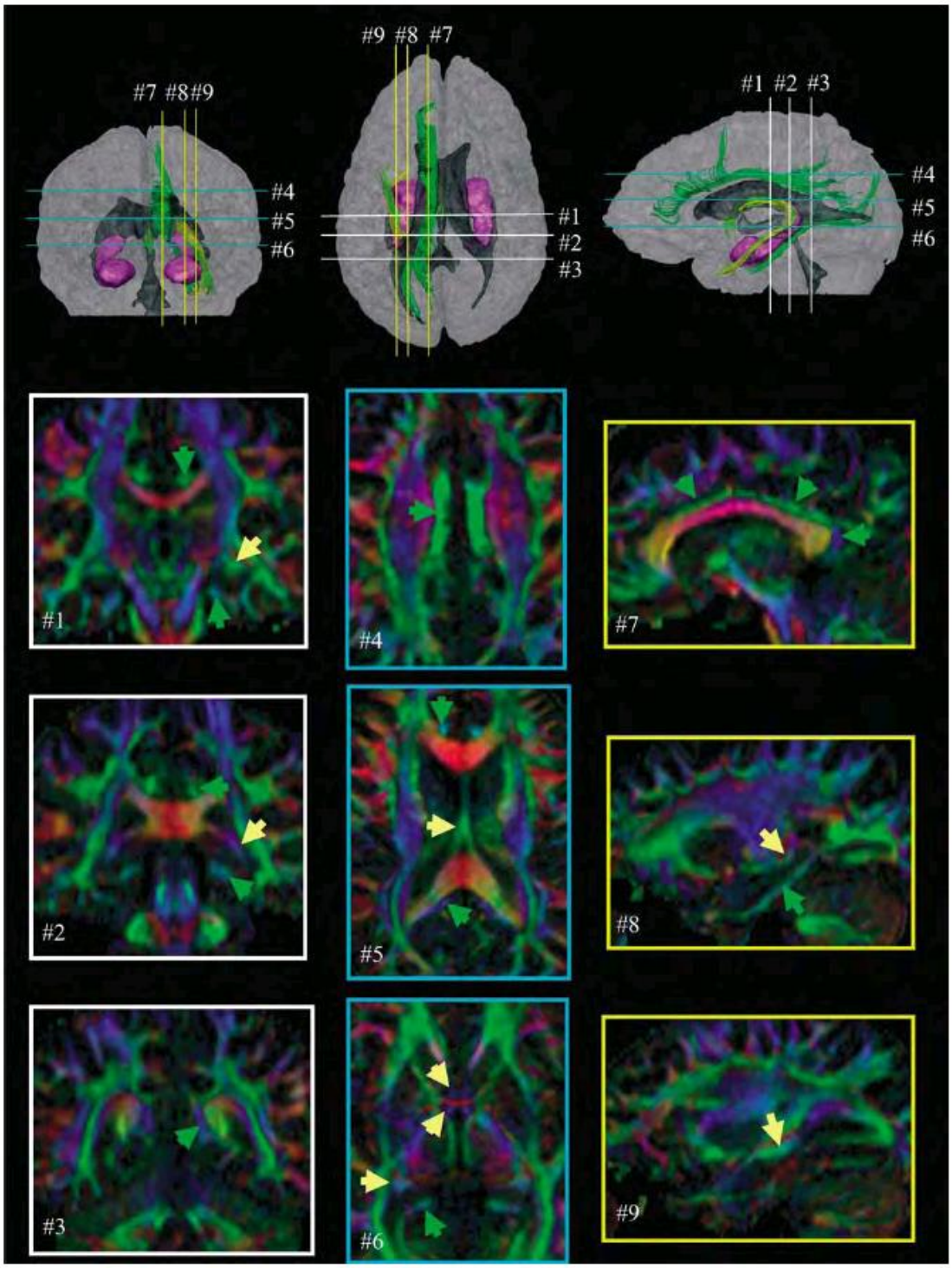

Figure 83. Trajectories of the cingulum (green) and fornix / stria terminalis (light yellow) and their identification in color maps at various slice levels and orientations. Locations of the 2D slices are indicated in the 3D panels. Ventricular system (gray) and hippocampus (purple) are also shown in the 3D reconstruction (Mori et al., 2005).

3(ix). Somatosensory

The somatosensory pathways represent two very specific pathways: the medial lemniscus and spinal lemniscus (Kamali et al., 2009).

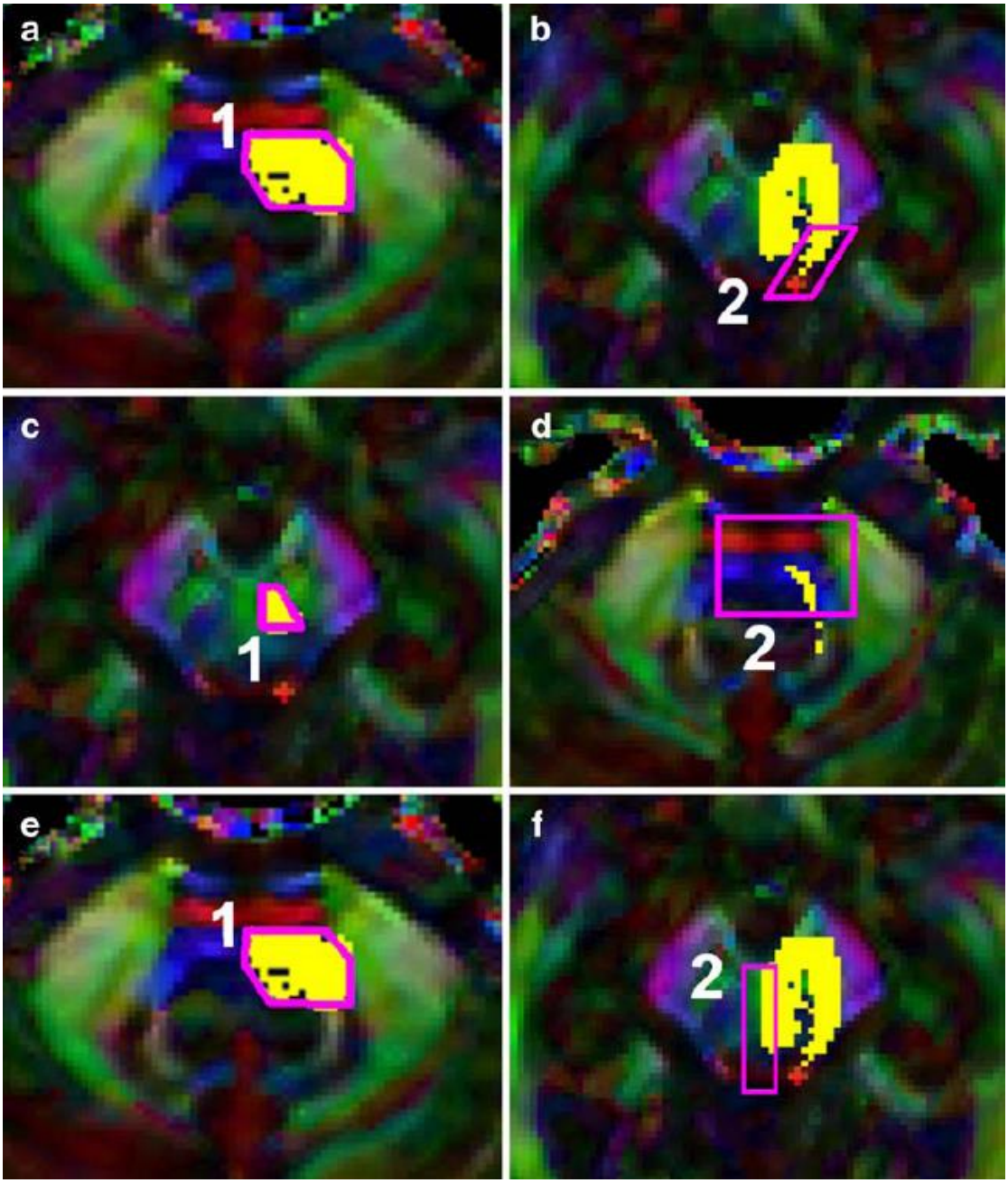

Figure 84. ROI locations used for reconstructions of the two sensory white matter tracts (a) and (b) ROIs for SL. (c) and (d) ROIs for ML. The ROIs are depicted in yellow on a DTI principal vector-coded map (red = right-left; green = anteriorposterior; blue = superiorinferior). The white pointer in (b) points at the tip of the tilted green area (TGA) on the DTI color-coded map where the ROI 2 for SL ends. The axial slices (b) and (c) are at the same

mesencephalic level and at the lowest axial level in which the red nuclei are visible on a T2-weighted map. The axial slices (a) and (d) are at the same axial level at the mid pons. (e) and (f) ROI locations used for reconstruction of the central tegmental tract (CTT). The axial levels for ROI 1 (e) and ROI 2 (f) described for CTT are at the same axial level as ROI 1 and 2 described for SL in (a) and (b). TGA: tilted green area; MGA: midline green area (Kamali et al., 2009).

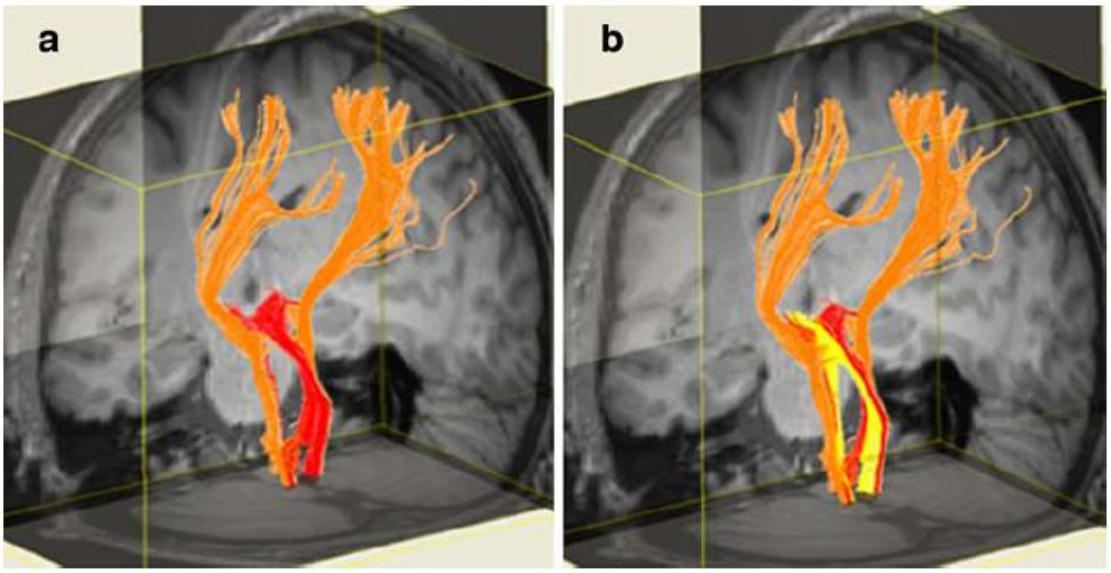

Figure 85. Three-dimensional view of reconstructed tracts using high spatial resolution (1 mm× 1 mm×1 mm) data (a) sensory tracts SL (orange), ML (red), (b) SL (orange), ML (red), CTT (yellow; Kamali et al., 2009).

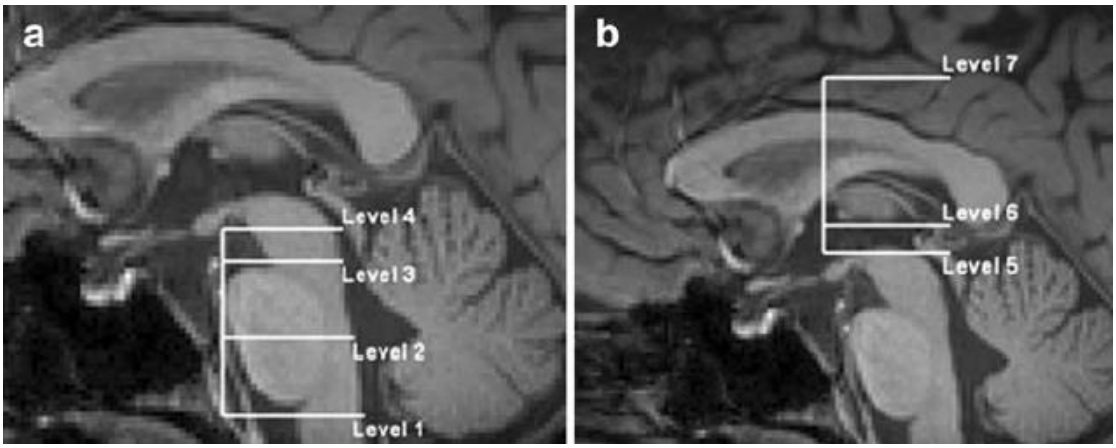

Figure 86. Structural (T1-weighted) MRI of the sagittal midline plane showing the different axial sections of (a) the brainstem and (b) supra-brainstem, the ML, SL, and CTT pathways of which are mapped in the following images (Kamali et al., 2009).

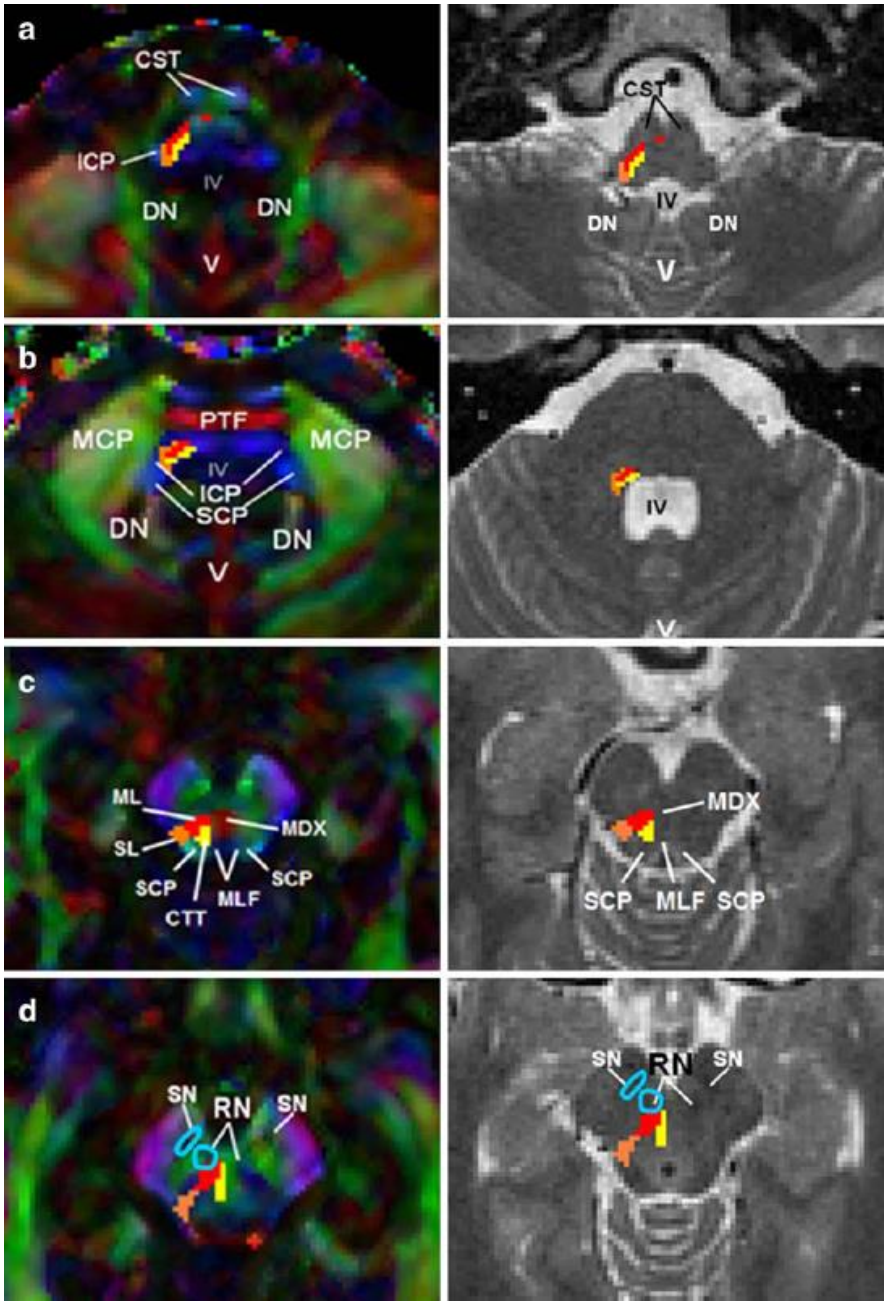

Figure 87. Mapping of the medial lemniscus (red), spinal lemniscus (orange), and central tegmental tract (yellow) in the brainstem in parallel to the concordant T2-weighted MR images (a) view at the upper medulla (corresponds to level 1 in Fig. 3a), (b) view at the mid-pons level (corresponds to level 2 in Fig. 3a), (c) view at the mesencephalic decussation (central red area on DTI color-coded map) at the lower mesencephalon (corresponds to level 3 in Fig. 3a), and (d) view at the lowest mesencephalic level, the red nuclei of which are visible in T2-weighted MR images (corresponds to level 4 in Fig. 3a). Well-delineated anatomical landmarks are labelled as follows: CST = corticospinal tract, DN = dentate nucleus, ICP = inferior cerebellar peduncle, IV = fourth ventricle, MDX = mesencephalic decussation, MCP = middle cerebellar peduncle, ML = medial lemniscus, PTF = pontine transverse fibers, SCP = superior cerebellar peduncle, SL = spinal lemniscus, V = vermis of the cerebellum (Kamali et al., 2009).

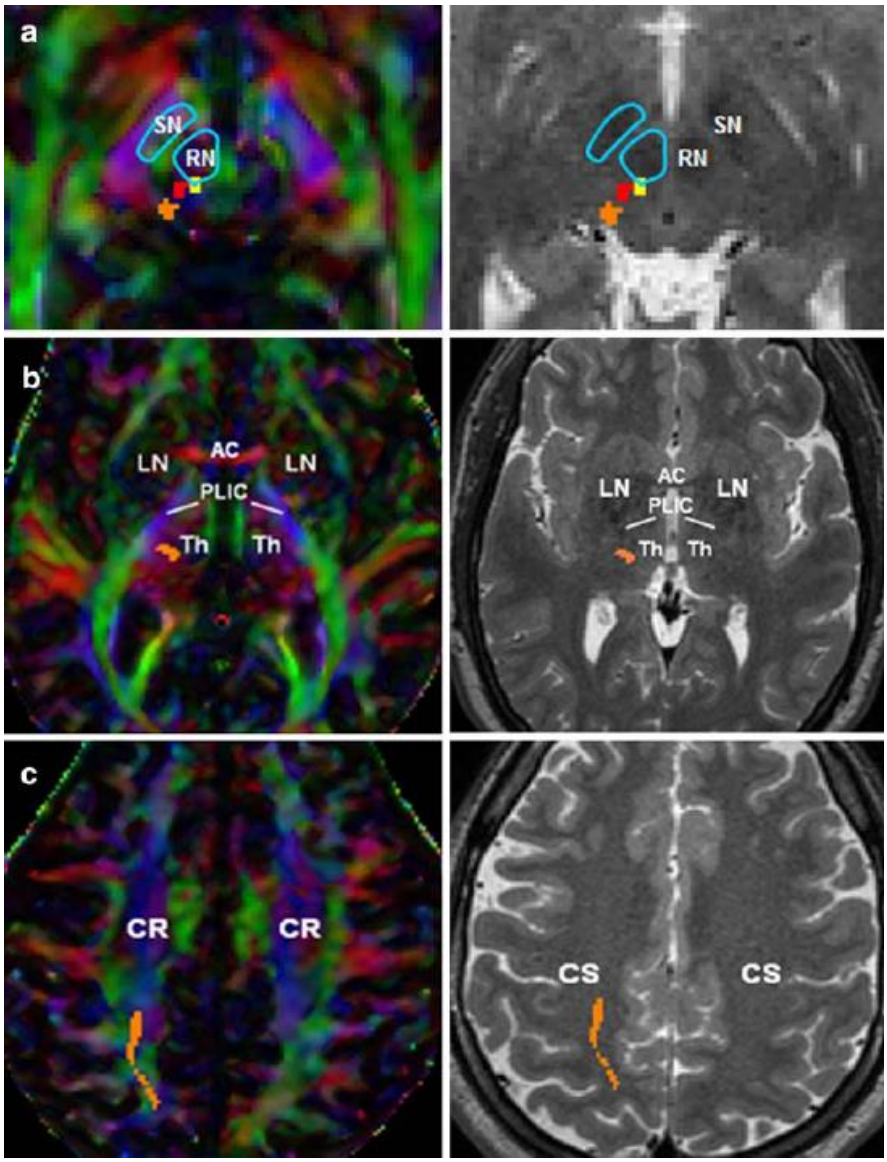

Figure 88. (a) Transverse DTI color-coded map and corresponding T2-weighted MR image for mapping the medial lemniscus (red), spinal lemniscus (orange), and central tegmental tract (yellow) at the mesencephalo-diencephalic level (corresponds to level 5 in Fig. 3b). (b) Transverse DTI color mapping and concordant T2-weighted MR image of SL at the diencephalon at the axial level in which the anterior commissure is visible (corresponds to level 6 in Fig. 3b). (c) Transverse DTI color-coded map and concordant T2-weighted image at the axial level corresponding to the cingulate sulcus showing cortical connections of the spinal lemniscus (corresponds to level 7 in Fig. 3b).Color coding is the same as in Fig. 2a, b. Well delineated anatomic landmarks are labelled as follows: AC = anterior commissure, CS = central sulcus, CR = corona radiata, LN= lentiform nucleus, PLIC = posterior limb of internal capsule, RN = red nucleus, SN = substantia nigra, Th: thalamus (Kamali et al., 2009).

4. Some examples of ROI seeding from the literature

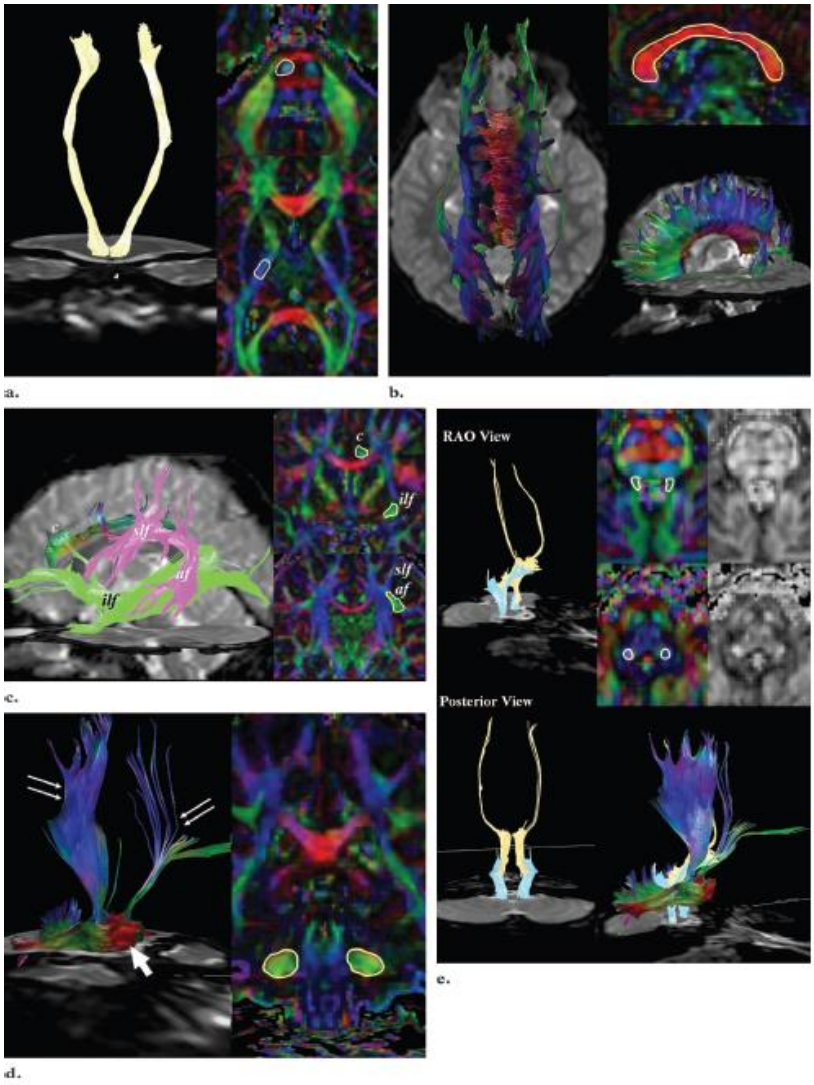

Figure 89. ROIs for generating FT images of the major white matter fiber tracts. (a) FT image of the corticospinal tract (left) is generated from the fibers connecting two ROIs in the longitudinal pontine fibers and the posterior limb of the internal capsule (right). (b) FT images of the CC (left and bottom right) are generated from a single ROI at the precise anatomic locations on the sagittal color map (top right). (c) FT image of longitudinal fiber bundles connecting anteroposteriorly (green fibers) (left) is generated from ROIs on coronal color maps (right). The SLF is connected to the AF; these fiber tracts are generated from a single ROI. Fiber tracts of other longitudinal fibers like the cingulum (c) and ILF are also generated from coronal images. (d) FT image of the middle cerebellar peduncles (left) is generated from single ROIs on the coronal view (right). These fiber tracts form a midline crossing by means of the red transverse pontine fibers (thick arrow), and some extend to cortical connections superiorly (thin arrows). (e) FT images of the superior (yellow) and inferior (blue) cerebellar peduncles (left and bottom right) are generated from single ROIs on axial color maps (top right). RAO = right anterior oblique (Lee et al., 2005).

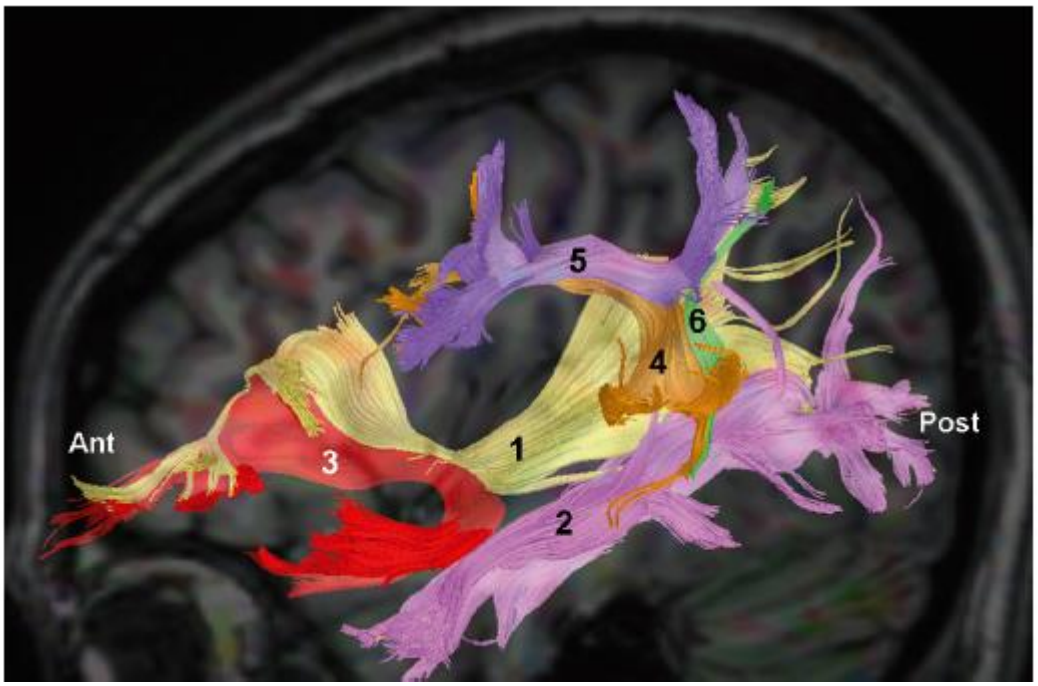

Figure 90. DTI tractography reconstruction of the association bundles of a left hemisphere. 1, IFOF; 2, ILF; 3, UF; 4, AF; 5, horizontal segment of the SLF; 6, vertical segment of the SLF. Ant, anterior; Post, posterior (Martino et al., 2011).

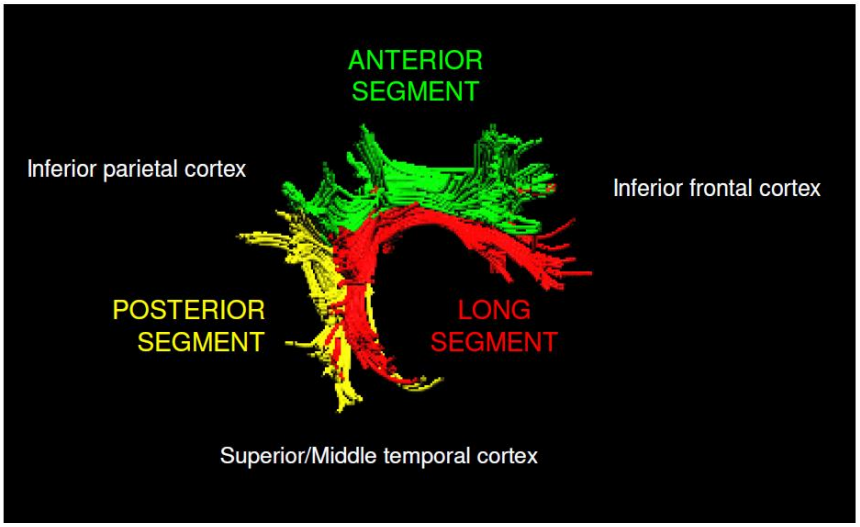

Figure 91. Averaged tractography reconstruction by using a two-region of interest approach. It shows a three-way connection between the superior temporal, inferior parietal, and the lateral frontal cortex. The direct

connection between the superior temporal and lateral frontal cortex is shown in red. The posterior segment of the indirect connection, running from the superior temporal to the inferior parietal cortex is shown in yellow. The anterior segment of the indirect connection, running from the inferior parietal to the lateral frontal cortex is shown in green (Gharabaghi et al., 2009).

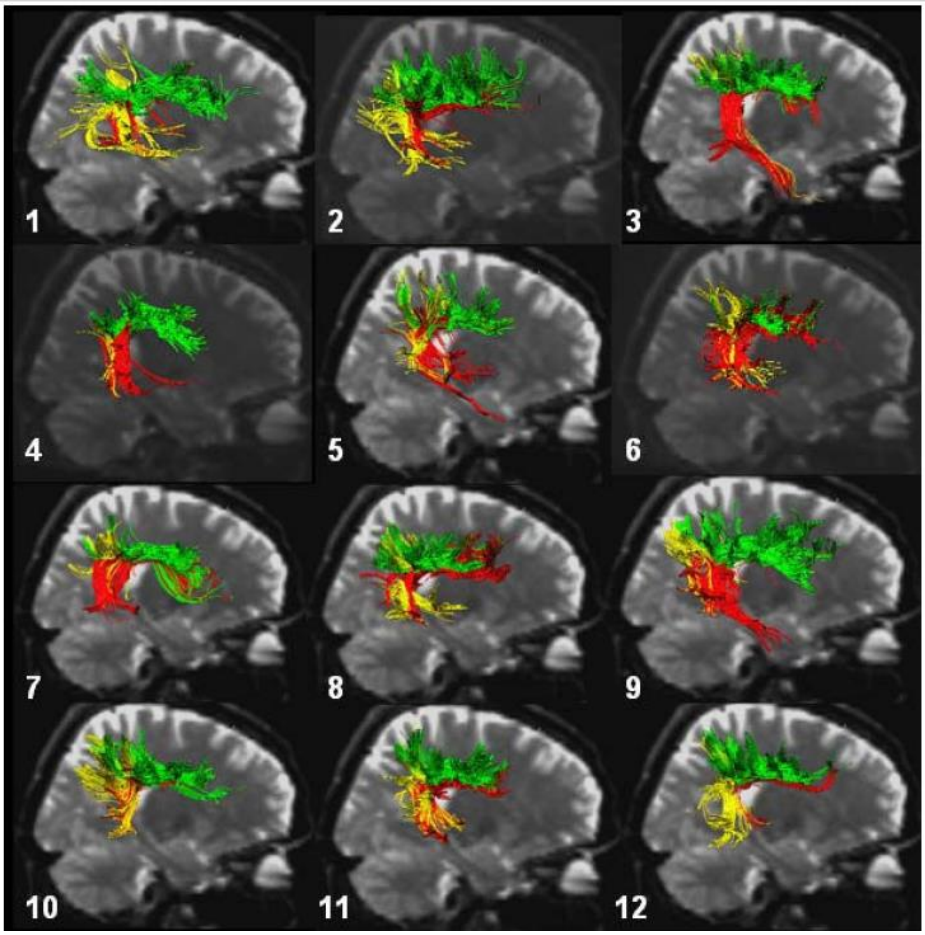

Figure 92. Reconstructed direct and indirect pathways (using a two-region of interest approach) in each of 12 healthy subjects. Reconstructions were superimposed on sagittal b0 data. Color coding as in Figure 91 (Gharabaghi et al., 2009).

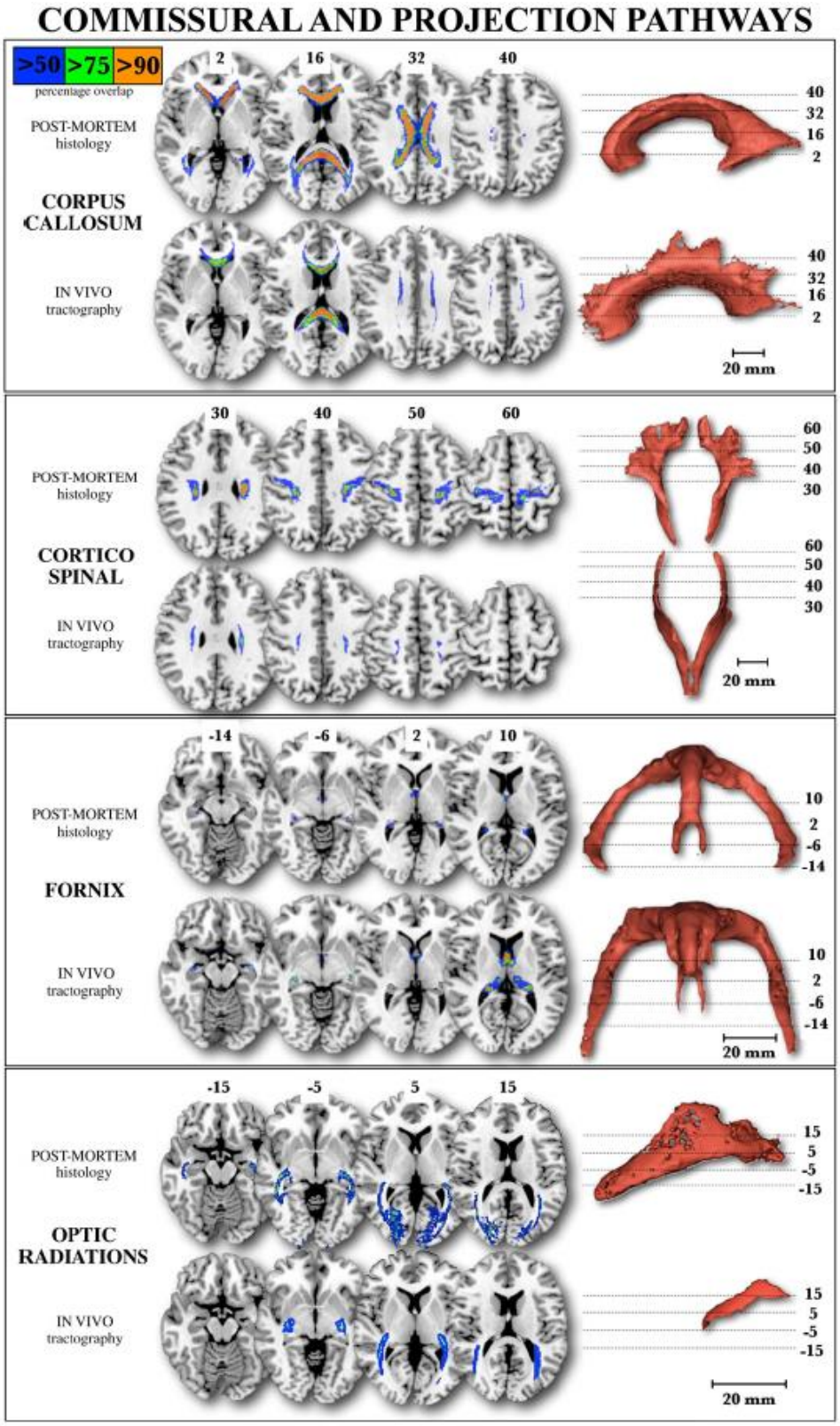

Figure 93. Comparison between percentage maps based on post-mortem histology (upper rows) (Bürgel et al., 2006) and DTI tractography (lower rows) of the major commissural and projection tracts (the anterior commissure was not available for the histological maps). Numbers above each slice refer to MNI co-ordinates.

On the right, tridimensional reconstructions of two sets of maps (N50% subjects' tract overlaps) are shown (de Schotten et al., 2011).

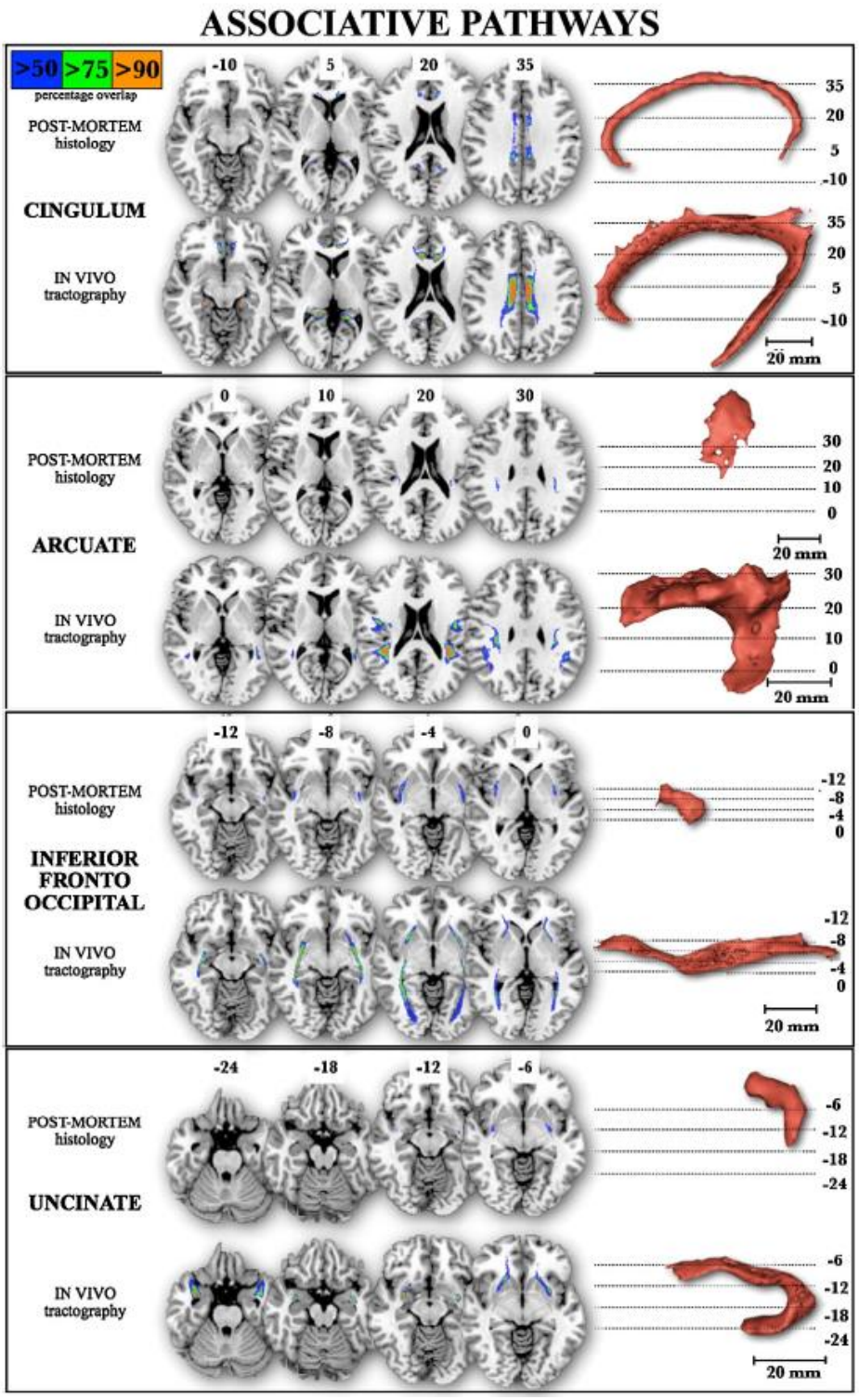

Figure 94. Comparison between percentage maps based on post-mortem histology (upper rows) (Bürgel et al., 2006) and DTI tractography (lower rows) of the major association tracts. Numbers above each slice refer to MNI co-ordinates. On the right, tridimensional reconstructions of two sets of maps (N50% subjects' tract overlaps) are shown (de Schotten et al., 2011).

References

Bürgel U, Amunts K, Hoemke L, Mohlberg H, Gilsbach JM, Zilles K (2006). White matter fiber tracts of the human brain: three-dimensional mapping at microscopic resolution, topography and intersubject variability. NeuroImage 29: 1092–1105.

DeJong RN. *The Neurologic Examination*. William Wesley Campbell, Russell N. DeJong, Armin F. Haerer (Eds). 6th Edition. Philadelphia Lippincott Williams & Wilkins, 2005.

Filler A. (2009). Magnetic resonance neurography and diffusion tensor imaging: origins, history, and clinical impact of the first 50,000 cases with an assessment of efficacy and utility in a prospective 5000-patient study group. Neurosurgery 65(4 Suppl):A29-43.

Gharabaghi A, Kunath F, Erb M, Saur R, Heckl S, Tatagiba M, Grodd W, Karnath HO. (2009). Perisylvian white matter connectivity in the human right hemisphere. BMC Neuroscience 3:13-15.

Jones DK, Cercignani M. (2010). Twenty-five Pitfalls in the Analysis of Diffusion MRI Data. NMR in Biomedicine 23:803–20.

Kamali A, Kramer LA, Butler IJ, Hasan KM. (2009). Diffusion tensor tractography of the somatosensory system in the human brainstem: initial findings using high isotropic spatial resolution at 3.0 T. European Radiology 19:1480-8.

Kaplan E, Naeser MA, Martin PI, Ho M, Wang Y, Baker E, Pascual-Leone A. (2010). Horizontal portion of arcuate fasciculus fibers track to pars opercularis, not pars triangularis, in right and left hemispheres: a DTI study. NeuroImage 52:436-44.

Lee SK, Kim DI, Kim J, Kim DJ, Kim HD, Kim DS, Mori S. (2005). Diffusion-tensor MR imaging and fiber tractography: a new method of describing aberrant fiber connections in developmental CNS anomalies. Radiographics 25:53-68.

Martino J, De Witt Hamer PC, Vergani F, Brogna C, de Lucas EM, Vázquez-Barquero A, García-Porrero JA, Duffau H. (2011). Cortex-sparing fiber dissection: an improved method for the study of white matter anatomy in the human brain. Journal of Anatomy 219(4):531-41.

Mori S, Wakana S, Nagae-Poetscher LM, van Zijl PC. (2005). MRI atlas of human white matter. Amsterdam, The Netherlands: Elsevier.

Pannek K, Mathias JL, Bigler ED, Brown G, Taylor JD, Rose S. (2010). An automated strategy for the delineation and parcellation of commissural pathways suitable for clinical populations utilising high angular resolution diffusion imaging tractography. NeuroImage 50:1044-53.

Schmahmann JD, Pandya DN, Wang R, Dai G, D'Arceuil HE, de Crespigny AJ, Wedeen VJ. (2007). Association fibre pathways of the brain: parallel observations from diffusion spectrum imaging and autoradiography. Brain 130(Pt 3):630-53.

de Schotten TM, Ffytche DH, Bizzi A, Dell'Acqua F, Allin M, Walshe M, Murray R, Williams SC, Murphy DG, Catani M. (2011). Atlasing location, asymmetry and inter-subject variability of white matter tracts in the human brain with MR diffusion tractography. NeuroImage 54:49-59.